International Journal of Earth Sciences
https://doi.org/10.1007/s00531-024-02415-9

ORIGINAL PAPER

Sedimentary environment and a development model for source rocks rich in the green alga *Pediastrum*: a case study of the paleogene anjihaihe formation in the junggar basin, northwest china

Miao Yu[1,2] · Gang Gao[1,2] · Xinying Zhao[1,2] · Miao Liu[1,2] · Wanyun Ma[3,4,5] · Youjin Zhang[1,2]

Received: 9 January 2024 / Accepted: 9 April 2024

Abstract
In this study, *Pediastrum* has been observed in the Anjihaihe Formation (E_{2+3a}) shale through organic petrology studies. Additionally, analyses of total organic carbon and rock pyrolysis (Rock–Eval) revealed that the E_{2+3a} shale predominantly comprises oil-bearing type I and II kerogen at a low-maturity stage. The organic matter (OM) in the shale is primarily contributed by *Pediastrum*, indicating excellent original hydrocarbon generation potential. Hydrous pyrolysis was conducted on a *Pediastrum*-rich sample, and the liquid product was analyzed using gas chromatography–mass spectrometry (GC–MS) of the saturated fraction. It was discovered that *n*-C_{27} might serve as a characteristic biomarker indicating *Pediastrum* development. During warm and humid climatic conditions, rivers transport significant amounts of freshwater and terrigenous organic matter (OM) into the lake, leading to an increase in felsic minerals and a relative decrease in carbonate minerals. This, in turn, reduces water salinity, resulting in a relative increase in the abundance of *Pediastrum*. Conversely, during earlier hot and arid climatic conditions, the input of terrigenous OM decreases, and evaporation leads to increased salinity. When the water's salinity exceeds the "salinity critical point", the Pediastrum content decreases. Finally, this study presents a formation and evolution model for the E_{2+3a} shale in the Junggar Basin.

Keywords Geochemistry · Petrology · *Pediastrum* · Paleoenvironment · Anjihaihe formation · Junggar basin

Introduction

Research on organic matter (OM) in source rocks has highlighted the importance of spores, pollen, algae, fungi, and other sources (Xia et al. 2020; Yuan et al. 2023). Long-term oil and gas exploration has led to the successive discovery of various algae in continental and marine strata (Song et al. 1995, Wang et al. 2001), which have made essential contributions to hydrocarbon formation (Demaison et al. 1980; Qin et al. 2007; Stein 2009). The OM enrichment during sedimentation is influenced by various factors, such as paleoclimate, paleowater depth, and paleosalinity (Doner et al. 2019). *Pediastrum* is a colonial green alga of the Hydrodictyaceae family (Geel 2001; Komarek 2001; Krzeszowska 2019), usually composed of 4, 8, 16, 32, 64, or 128 cells in a thick layer of flat disc-shaped aggregates (Zhao et al. 2021). *Pediastrum* is widely distributed globally (Sun et al. 1987; Geel et al. 1996; Komarek 2001; Geel 2001) and its sensitivity to climate change makes it a valuable bioindicator for paleoclimate studies (Geel 2001). The appearance and abundance changes of *Pediastrum* are often used to infer variations in water salinity and depth during the depositional period, which, in turn, can be used to infer the climate and temperature changes at that time (Whitney et al. 2012). Following a euthermic algal distribution, *Pediastrum* can develop at 4–36 ℃ (Wang et al. 1994). Some studies have suggested that *Pediastrum* is abundant in freshwater lakes and wetlands (Xiao et al. 1996; Jiang et al. 2006) and that

✉ Gang Gao
gg_2819@163.com

1 College of Geosciences, China University of Petroleum, Beijing 102249, China

2 National Key Laboratory of Petroleum Resources and Engineering, Beijing 102249, China

3 Research Institute of Experimental Testing, Xinjiang Oilfield Company, PetroChina, Karamay 834000, China

4 Xinjiang Conglomerate Reservoir Laboratory, Karamay 834000, China

5 Development of Conglomerate Reservoirs, Key Laboratory of Exploration, Karamay 834000, Xinjiang, China

Published online: 25 April 2024

the increased *Pediastrum* content indicates decreased water salinity (Zamaloa and Tell 2005; Brenner et al. 2006; Wan et al. 2008). However, some other studies have emphasized that increased *Pediastrum* content indicates decreased lake level or shallower waters (Zheng et al. 2003; Jiang et al. 2013). In other words, an increase in *Pediastrum* content is accompanied by an increase in water salinity (Zhu et al. 1978; Lamb et al. 1999; Sylvestre 2002; Gosling et al. 2009).

While recognized as a significant lacustrine source rock in the Junggar Basin, there are limited studies available on the E_{2+3a} shale, particularly regarding its geochemical characteristics and sedimentary environment (Ma et al. 2020). According to Chen et al. (2019), the oil and gas formation potential of the E_{2+3a} shale members is limited due to the low abundance and maturity of the organic matter (OM). Consequently, the level of research conducted on this shale is relatively low, and studies regarding its sedimentary environment and primary OM content are contentious. Zhou et al. (2012) proposed that the OM of the E_{2+3a} shale is predominantly composed of *Pediastrum* and Dinoflagellate, suggesting the possibility of a transgressive event in the lake basin's history. In contrast, Zhu et al. (2022) suggested that Dinoflagellate serves as the main producers of OM, deposited in freshwater lacustrine facies. Wang et al. (2021) suggested that the E_{2+3a} shale was primarily deposited under continental brackish water conditions, without conducting OM analysis. Conversely, Wang et al. (2019) linked the E_{2+3a} shale to a continental saline lake basin based on their study of dolomite genesis. Yu et al. (2023) proposed that the OM in the E_{2+3a} shale is mainly composed of *Pediastrum* and possesses excellent hydrocarbon generation potential. However, systematic analysis of the developmental environment of its high-quality shale has not yet been conducted. The aforementioned studies on OM were limited to the microscopic examination of kerogen and they did not involve its characteristic biomarkers. Therefore, based on the geochemical characteristic analysis of the E_{2+3a} shale, this study focused on the main OM of the E_{2+3a} shale, its characteristic biomarkers, and its development model.

Geological settings

The Junggar Basin, which has been proven to be abundant in hydrocarbon resources, is located in northwest China (Bai et al. 2016; Xu et al. 2017; He et al. 2019). The basin has experienced four stages of evolution: pre-Carboniferous basement formation, Carboniferous-Permian further development, Mesozoic Paleogene inland lake basin and Neogene Quaternary intense compression, and consists of six primary structural units at present (Fig. 1a) (Tang et al. 2022; Tian et al. 2022).

The Ziniquanzi Formation (E_{1+2z}) comprises a rich variety of sedimentary facies, including alluvial fan, fluvial, and fan delta deposits. In contrast, the Anjihaihe Formation (E_{2+3a}) is characterized by the presence of stable lacustrine fine-grained deposits, indicative of a tranquil lake environment (Qin et al. 2014; Yu et al. 2023). During the E_{1+2z} sedimentary period, the lithology predominantly consisted of oxidized mudstone (Wang et al. 2020). Conversely, in the stable tectonic environment of the E_{2+3a} period, a set of gray-green, greenish-gray, and gray-black shales was deposited. (Wang et al. 2020; Yu et al. 2022) (Fig. 1b). Since the Neogene, E_{2+3a} in the northern part of the basin has suffered strong denudation, with the E_{2+3a} depositional center being at the southern margin of the central depression and the piedmont thrust belt (Fig. 1a).

Sampling and methods

This study is an extension of the study by Yu et al. (2023) on *Pediastrum* and mainly focuses on the characteristic biomarkers of *Pediastrum* and its enrichment mechanism. In addition to the samples analyzed by Yu et al. (2023), this study included additional samples and conducted supplementary tests. The samples analyzed in this study, as well as those by Yu et al. (2023), were processed in the same batch, ensuring comparability of the data. All 69 samples were collected from the E_{2+3a} shale, including eight outcrop samples from the Anjihaihe outcrop (44° 62′ N, 85° 61′ E) (Fig. 1a, c, and d), nine core samples from well DS, and fifty-two cutting samples from wells Fw and Tw (Fig. 1a).

All the samples were analyzed for organic petrology, total organic carbon (TOC), and rock pyrolysis (Rock–Eval). Initially, each sample was crushed to a particle size smaller than 0.2 mm. Approximately 100 mg of the samples were treated with a 5% dilute hydrochloric acid solution, followed by thorough rinsing with distilled water. Subsequently, the samples were dried at 60 °C oven for a duration of 12 h. The determination of Total Organic Carbon (TOC) content was conducted using a LECO CS-230 carbon and sulfur analyzer. Pyrolysis parameters were established using an OGE-II workstation at similar conditions, with an initial temperature of 300 °C. The temperature was incrementally raised to 600 °C under inert conditions, utilizing nitrogen as the carrier gas, at a heating rate of 25 °C/min. A Leica DM4500P/DFC450C optical microscope was used in the experiment. The mineral composition of 25 samples was observed, and their organic maceral components were quantitatively analyzed. Quantification was performed based on an image processing method, using no fewer than 30 photos for each sample, The specific operational method follows the description provided by Xie et al. (2013).

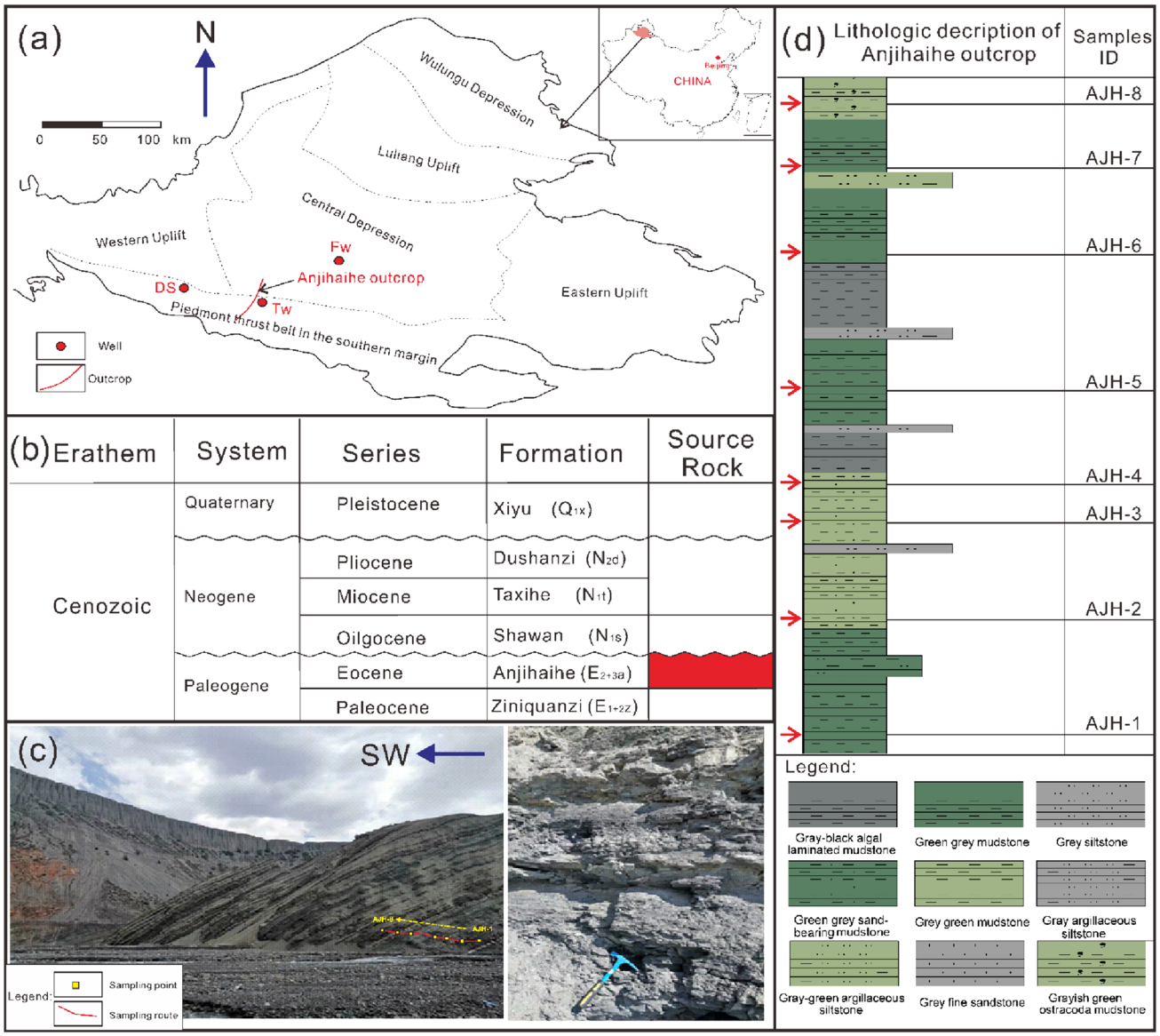

Fig. 1 **a** Geologic map of the Junggar Basin. **b** Stratigraphic column of the Cenozoic of the Junggar Basin. **c** Sampling photo of Anjihaihe outcrop. **d** Lithological description and sampling points of Anjihaihe outcrop. Note: "AJH-1"- "AJH-8", ID of outcrop samples

Seventeen outcrops and core samples were selected for scanning electron microscopy (SEM) and energy-dispersive spectroscopy (EDS) analysis. The sample utilized for SEM and EDS analyses was a small core fragment. The surface underwent polishing using argon ions, and a layer of Au was plated to enhance conductivity. SEM analysis was conducted using an FEI Quanta 200F instrument. OM and typical minerals were analyzed employing an EX-250 energy spectrometer. Trace element analysis were conducted on eight outcrop samples. The trace element contents of the samples were tested and analyzed under standard temperature and humidity conditions utilizing a NexION300D plasma mass spectrometer. Detection methods and standards adhered to GB/T 14506.30–2010. Whole-rock X-ray diffraction (XRD) were conducted on eight outcrop samples. The mineral composition serves as a crucial foundation for analyzing rock deposition and diagenesis, playing a vital role in investigations within these domains. For this purpose, a Rigaku TTR multifunctional X-ray diffractometer was utilized, operating at a scanning rate of 2°/min (2θ) and covering a scanning range of 5–45° (2θ).

Hydrous pyrolysis was performed on AJH-4 and the reaction residue, expelled oil, and residual oil were obtained. The size and weight of the sample for hydrous pyrolysis were consistent with those in Yu et al. (2023). The sample was heated to the set temperature at 2 ℃/min using a

GPM-3 hydrocarbon generation simulator and kept constant for 24 h. The set temperatures were 280, 300, 330, 350, 370, and 500 °C. Liquid hydrocarbons obtained directly from the reactor, while residual oil was obtained by crushing the samples and Soxhlet extraction. The expelled oil, residual oil, and outcrop samples were analyzed using gas chromatography–mass spectrometry (GC–MS). An Agilent 7890-5975c gas chromatographer–mass spectrometer was performed on GC–MS analysis, and the analysis method and procedure of GC–MS are consistent with those described in Yu et al. (2023). The instrument was outfitted with an HP-5MS fused silica column, with the carrier gas being 99.999% helium at a flow rate of 1 mL/min. Initially, the column temperature was maintained at 50 °C for 1 min. Subsequently, the temperature was ramped up to 120 °C at a rate of 20 °C/min, then to 250 °C at a rate of 4 °C/min, and finally to 310 °C at a rate of 3 °C/min, where it remained for 30 min. Vitrinite reflectance (%Ro) was measured for 28 samples and the hydrous pyrolysis reaction residue of sample AJH-4. The %Ro measurements were conducted using an MSP400 microfluorescence spectrometer. Reflected vertical incident light on the vitrinite surface was measured employing an oil-immersed objective lens. Comparison of reflected light intensities was performed under identical conditions. Each sample was analyzed at a minimum of 30 points.

Results

Organic geochemical characteristics

The TOC contents of the E_{2+3a} shale were distributed in the range of 0.21–2.70% (avg. 0.88%) (Table S1). The S_1, S_2, and S_1+S_2 Rock–Eval values were in the ranges of 0.07–0.86 mg/g (avg. 0.18 mg/g), 0.19–16.98 mg/g (avg. 3.57 mg/g), and 0.27–17.22 mg/g (avg. 3.75 mg/g), respectively (Table S1). Although the samples were highly heterogeneous, they were primarily fair- to good-quality source rocks (Peters and Cassa 1994) (Fig. 2a). The hydrogen index (HI) was used to evaluate the type of OM (Liu et al. 2018; Zhang et al. 2020). The HI values of the E_{2+3a} shale samples ranged 36–763 mg HC/g TOC (avg. 359 mg HC/g TOC) (Table S1). In the HI–TOC cross plot, most of the E_{2+3a} shale samples fall in the "fair- to good-oil source rock" area and some of the samples fall in the "gas/oil source rock" area (Tissot and Welte 1984), which indicates a strong oil-generating capacity (Fig. 2b). The pyrolysis Tmax temperatures were in the range of 312–443 °C, with an average of 424 °C (Table S1) (Samples showing a Tmax value below 300 °C, indicating a low organic content insufficient to determine accurate Tmax, were excluded from the analysis), indicating low thermal maturity. The %Ro ratios ranged from 0.43% to 0.77%, with an average of 0.66% (Table S1), indicating that the majority of shale samples from E_{2+3a} were in the immature to low mature stages. In addition, the kerogen types of the E_{2+3a} shale samples were mainly types I and II (Fig. 3) (Mukhopadhyay et al. 1995). Moreover, it is noted that the OM abundance and type of outcrop samples generally

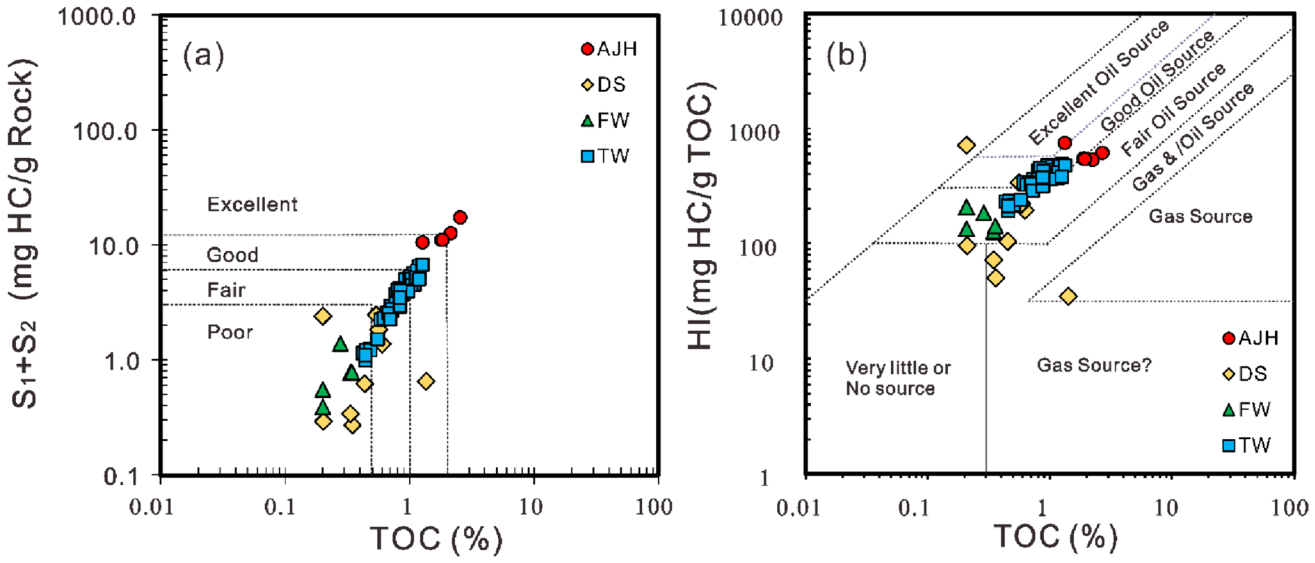

Fig. 2 **a** Cross plot of S_1+S_2 versus TOC (according to Peters and Cassa 1994). **b** Cross plot of TOC versus HI (according to Tissot and Welte 1984)

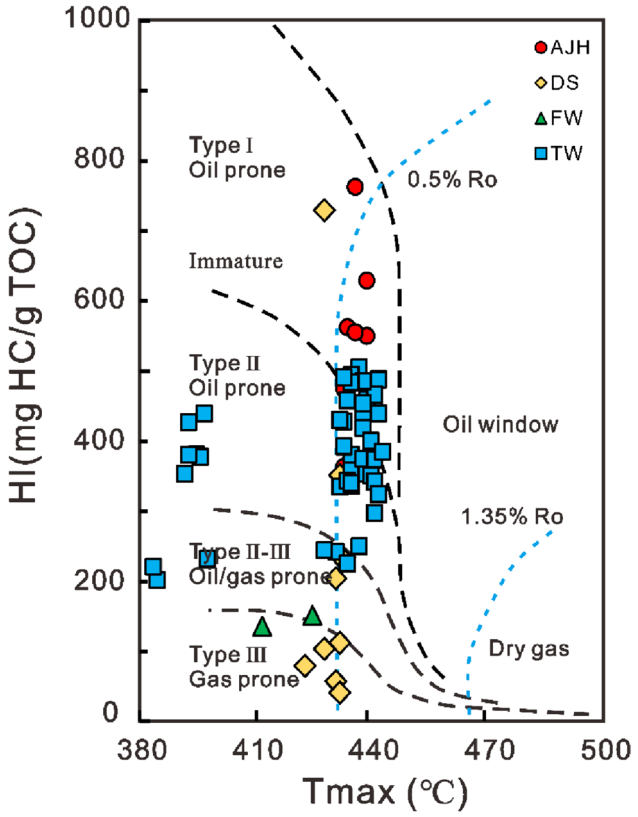

Fig. 3 Cross plot of HI versus Tmax of the E_{2+3a} shale samples (according to Mukhopadhyay et al. 1995)

outperform those of drilled samples. For instance, in the TW well, certain non-source rocks exhibit extremely low Tmax values, while samples from the DS well display notably low OM abundance, predominantly comprising type III kerogen. This discrepancy may be attributed to the proximity of the outcrop to the E_{2+3a} deposition sites during the relevant period, whereas current drilling activities are primarily situated at the sedimentary periphery of the formation. Consequently, deploying drilling wells to the sedimentation center may lead to closer access to the high-quality shales of the E_{2+3a}.

Petrological characteristics

The thin sections and SEM observation revealed the presence of *Pediastrum* in the E_{2+3a} shale (Fig. 4a–c). *Pediastrum* is widely distributed, generally star-shaped, with a clear cell structure, and exists with approximately 20 cells, of which, each outer cell has two projections. The cell color of *Pediastrum* is yellow-green and the diameters of the algae are generally larger than 30 μm (Fig. 4c). The high S value in the energy spectrum may be related to the presence of C–S complexes (Fig. 4d).

The content of *Pediastrum* in the samples ranged from approximately 0.55% to 6.30% (avg. 2.65%). Furthermore, the *Pediastrum* content in outcrop samples generally exceeded that found in drilling samples, aligning with the results of organic geochemical analysis. (Fig. 5). Due to the different sedimentary environments of the source rocks, the contents of *Pediastrum* vary widely among the samples (Stach et al. 1982). The TOC content and $S_1 + S_2$ are positively correlate with the abundance of *Pediastrum* (Fig. 5a and b), which indicates that the *Pediastrum* contributes notably to the OM of the E_{2+3a} shales. Therefore, the favorable depositional conditions and paleoenvironment leading to the development of *Pediastrum* and thus the highest potential hydrocarbon generating sections of the E_{2+3a} shale must be determined crucially.

Mineralogical characteristics

The mineral composition was mainly clay, ranging 58.70–67.7% (avg. 63.45%). The clay minerals were mainly illite and smectite, with contents 20.00–39.00% (avg. 29.60%) and 36.00–65.00% (avg. 53.00%), respectively. The contents of kaolinite and chlorite were low, 6.00–17.00% (avg. 10.40%) and 5.00–9.00% (avg. 7.00%), respectively. The quartz, potassium feldspar, plagioclase, calcite, and pyrite content ranges were 18.10–28.10% (avg. 22.60%), 0.80–1.70% (avg. 1.20%), 2.60–7.10% (avg. 3.70%), 1.80–5.50% (avg. 3.40%), and 3.00–5.20% (avg. 4.10%), respectively (Table 1). Thin-section observation provides the most intuitive method to analyze rock structure and composition (Pan et al. 2020). High content of carbonate minerals was not conducive of the development of *Pediastrum* (Fig. 6a–c). The limited development of carbonate was accompanied by a high content of clay minerals, and *Pediastrum* appeared to be more abundant (Fig. 6d–f).

Trace element characteristics

A total of 48 trace elements were analyzed (Table 2), and the relative contents and ratios varied significantly among different samples, indicating the strong heterogeneity of the shale. The Sr/Ba values were observed to vary from 0.53 to 1.38 (avg. 1.01), the Sr/Cu values from 4.76 to 15.25 (avg. 10.51), and the Rb/Sr values from 0.2 to 0.6 (avg. 0.34). Further, V/(V + Ni) values were in the range of 0.6–0.68 (avg. 0.64), Fe/Mn values, 55.56–95.47 (avg. 80.66), δU (δU = 2U/(U + Th/3) values, 0.86–1.29 (avg. 1.03), Zr/Rb values, 0.86–1.13 (avg. 0.99), Mo/TOC values, 1.56–4.65 (avg. 3.12), Ni/Co values, 0.79–7.04 (avg. 2.64), Mn/Ti values, 0.10–0.17 (avg. 0.13), and the Cu/Ti values, 0.009–0.011 (avg. 0.010).

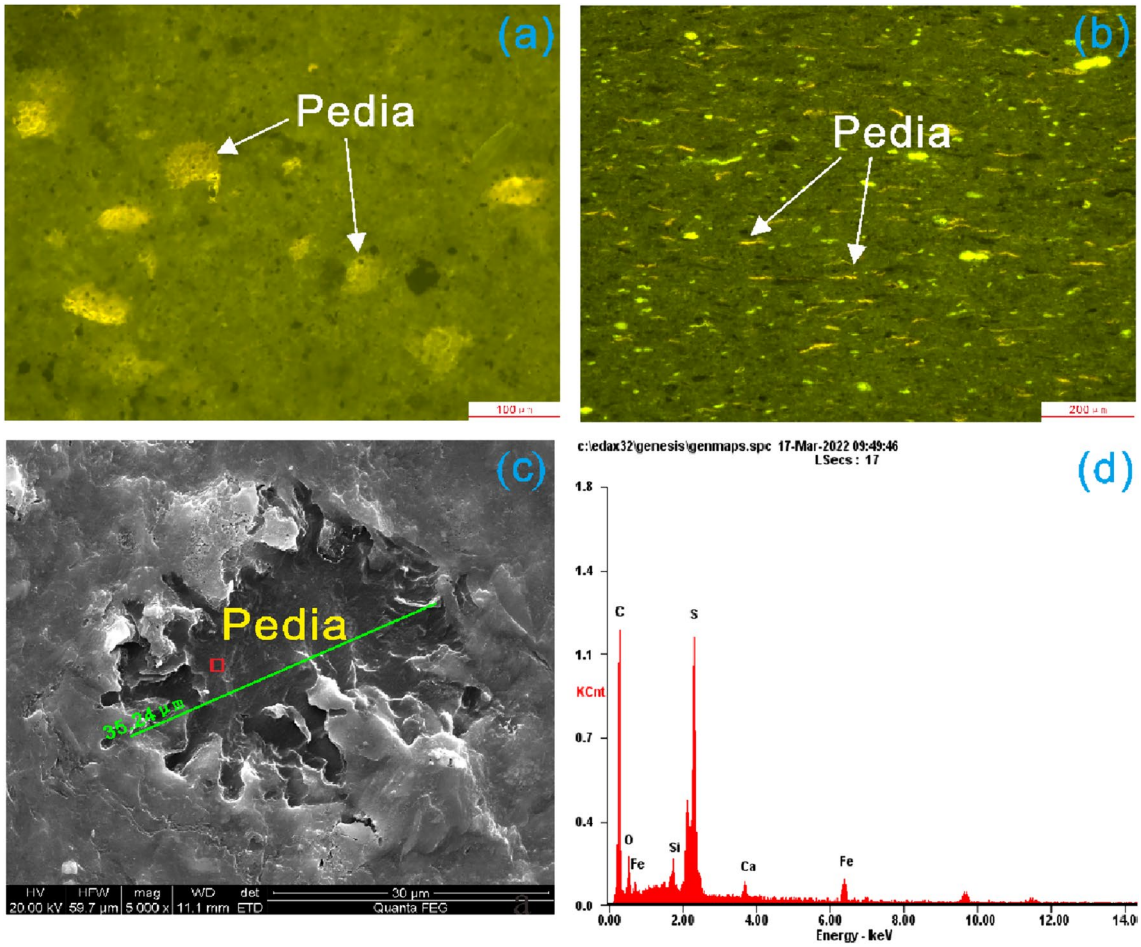

Fig. 4 Organic macerals and SEM images of samples. **a** Fluorescence image of the AJH-1 samples along the bedding direction; the clear structure of *Pediastrum* is evident. **b** Fluorescence image in the vertical bedding direction of the AJH-1 sample, showing the lamellar distribution of *Pediastrum*. **c** SEM image of the AJH-4 sample and diameter of a single *Pediastrum* being larger than 30 µm. **d** EDS image of the sample AJH-4 and the selected measuring point shown in Fig. 2c. Abbreviations: Pedia, *Pediastrum*

Aliphatic hydrocarbon characteristics of the extracts

The distribution characteristics of the carbon number and the ratio of the related parameters of *n*-alkanes are effective means of studying the origin and maturity of OM (Grantham and Wakefield 1988). The carbon number distribution of *n*-alkanes in the samples mainly ranged from *n*-C_{16} to *n*-C_{33}. Among them, all the *n*-alkane samples exhibited the primary carbon peak of *n*-C_{27} (Fig. 7a–d), and the relative content of *n*-C_{27} ranged 27.74–34.79% (avg. 32.19%). Pristane and phytane were detected in every sample. The values of Pr/Ph, Pr/*n*-C_{17}, and Ph/*n*-C_{18} ranged between 0.59–1.02 (avg. 0.77), 0.25–0.51 (avg. 0.36), and 0.25–0.87 (avg. 0.51), respectively (Table 3). In the m/z = 191 chromatogram, tricyclic terpanes exhibited a lower abundance than pentacyclic terpanes. The Ts values were significantly lower than Tm, with Ts/Tm ranging 0.021–0.047 (avg. 0.034). In addition, Gammacerane/C_{30}hopane (G/C_{30}H) ranged 0.15–0.50 (avg. 0.28) (Fig. 8a, c, e, and g). The regular steranes, C_{27}ααα(20*R*) sterane and C_{29}ααα(20*R*) sterane, were of asymmetric "V" type (Fig. 8b, d, f, and h).

According to the liquid hydrocarbon (expelled and residual oil) GC–MS results, regardless of the expelled or residual oil, the dominant carbon peak of saturated hydrocarbon gradually decreased with an increasing degree of thermal evolution (Figs. 9 and 10), and the relative concentration of *n*-C_{27} gradually decreased. The tricyclic terpene content was very low in the unheated samples (Figs. 9 and 10), and it gradually increased during thermal evolution (Figs. 9 and 10). The distribution of regular steranes did not change with increasing maturity (Figs. 9 and 10).

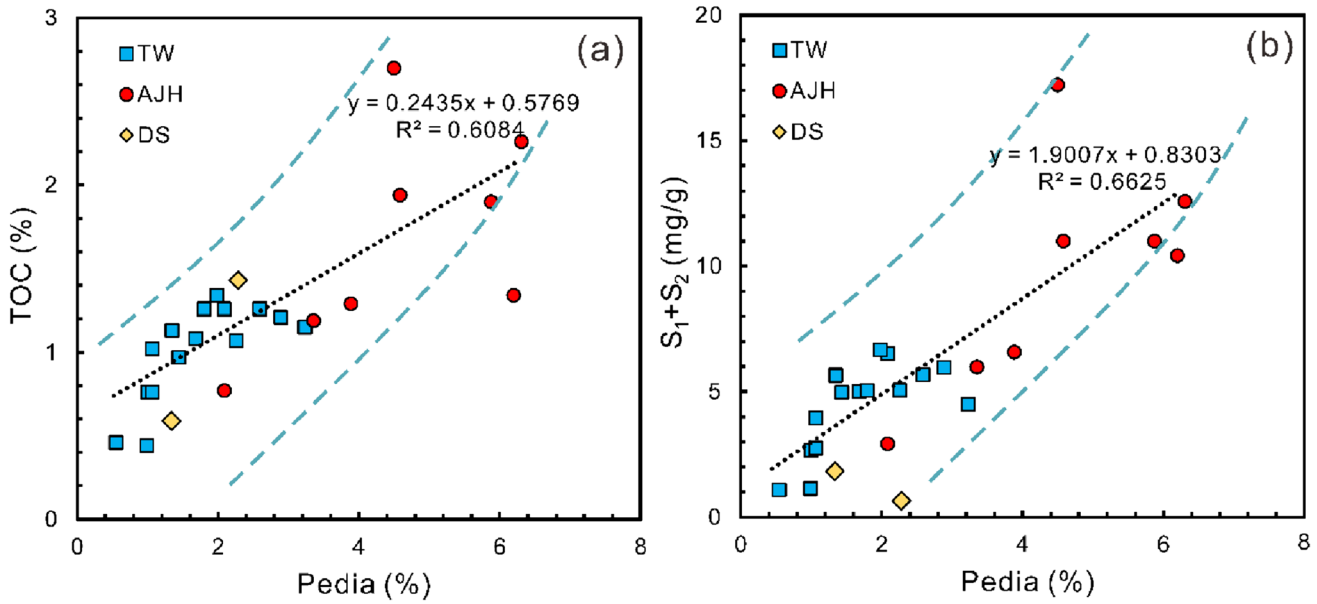

Fig. 5 **a** Cross plot of the TOC content versus the *Pediastrum* content. **b** Cross plot of S_1+S_2 versus the *Pediastrum* content. Abbreviations: Pedia, *Pediastrum*

Table 1 Mineral composition of the E_{2+3a} shale samples, Junggar Basin

Samples	Carbonate minerals	Felsic minerals	Clay minerals	Illite Smectite	Illite	Kaolinite	Chlorite
AJH-1	10.6	23.2	62.5	57	30	8	5
AJH-2	4.9	25.1	61.7	65	20	6	9
AJH-3	5.5	22.6	67.7	59	29	7	5
AJH-4	4.1	25.1	66.9	57	29	8	6
AJH-5	2.7	26.6	65.5	36	39	17	8
AJH-6	2	33.3	60.8	49	31	12	8
AJH-7	1.8	30.4	63.8	54	26	13	7
AJH-8	2.9	33.2	58.7	47	33	12	8

Discussion

Biological precursors

OM in lacustrine mudstones is typically dominated by aquatic algae and bacteria (Brocks et al. 1999). Simulation experiments conducted on the algal hydrocarbon-generation ability show that it can be classified into two types: strong and weak hydrocarbon-generation ability (Wang et al. 1994). Algae with high hydrocarbon generating capacity are primarily planktonic cyanobacteria and green algae (Sherwood 1991), whereas algae with poor hydrocarbon-generation ability are majorly benthic algae, which develop rhizoids and are rooted in soft silt (Wang et al. 1994). Low-chain length n-alkanes ($<C_{19}$) are assumed to be derived from lower aquatic organisms, such as planktonic algae and bacteria; mid-chain length *n*-alkanes (*n*-C_{20}–*n*-C_{26}) indicate the contribution of aquatic plants and long-chain length *n*-alkanes ($>C_{27}$) reflect the contribution of higher terrestrial plants (Riboulleau et al. 2007; Kristen et al. 2010; Kirellos et al. 2017). However, some studies suggested that long-chain length *n*-alkanes may indicate the contribution of algae; for example, *n*-C_{27} may indicate the contribution of Botryococcus braunii (Liao et al. 2022) and green algae can cooperate with *n*-C_{27} in long chains (Zhang et al. 2015). In other words, *n*-C_{27} is easily affected by lake hydrological changes, whereas a long-chain length in *n*-alkanes can directly indicate terrigenous contributions (Liu et al. 2016).

The relative content of *n*-C_{27} exhibits some correlation with the abundance *Pediastrum* (Fig. 11a). In addition, with increasing maturity, the peak type of *n*-alkanes changed from the posterior peak to the anterior peak, however, the

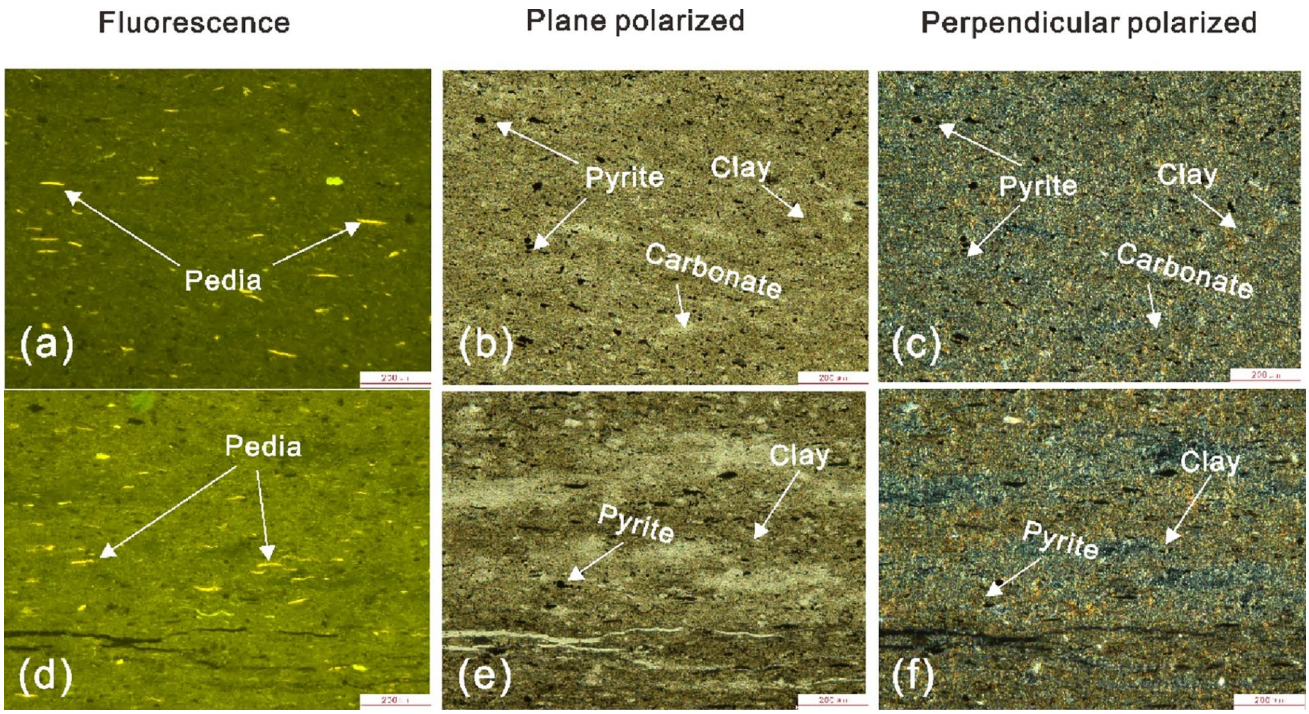

Fig. 6 Microscopic images of the E_{2+3a} mineral composition. **a–c** is from sample AJH-1, *Pediastrum* is moderately developed, with high carbonate content, high clay mineral content, and a small amount of pyrite. **d–f** is from sample AJH-4, *Pediastrum* is developed with high clay mineral content and a small amount of pyrite. Abbreviations: Pedia, *Pediastrum*

Table 2 Trace element ratios of the E_{2+3a} shale samples, Junggar Basin

Samples	Sr/ cu	Fe/ Mn	Rb/ Sr	Sr/ Ba	Zr/ Rb	Mo/ TOC	Mn/ Ti	Mn/Fe	V/ V + Ni	δu	Cu/Ti
AJH-1	15.25	55.56	0.20	1.35	1.02	1.56	0.1039	0.0111	0.62	1.15	0.0109
AJH-2	9.16	93.50	0.39	0.87	1.13	2.41	0.0979	0.0105	0.68	0.89	0.0096
AJH-3	13.26	89.51	0.25	1.21	1.13	2.95	0.1455	0.0147	0.64	1.29	0.0103
AJH-4	7.42	77.76	0.43	0.71	1.06	4.65	0.1386	0.0132	0.60	0.95	0.0100
AJH-5	6.29	75.73	0.43	0.75	0.91	1.96	0.1108	0.0129	0.64	0.86	0.0105
AJH-6	13.18	67.85	0.20	1.31	0.90	3.52	0.1408	0.0112	0.62	1.09	0.0107
AJH-7	4.76	95.47	0.60	0.53	0.86	4.44	0.1310	0.0107	0.66	0.93	0.0096
AJH-8	14.76	89.91	0.21	1.38	0.91	3.45	0.1655	0.0180	0.67	1.06	0.0092

Note: δu, 2 U/ (U + Th/ 3)

main carbon peak remained to be *n*-C_{27} (Figs. 9 and 10). The relative content of *n*-C_{27} decreased gradually 31.44%–9.96%, which may be due to the fracturing of long-chain length *n*-alkanes during hydrocarbon generation and the expulsion of hydrocarbons (Derenne et al. 1992). Therefore, it is highly likely that the relative content of *n*-C_{27} reflects the contribution of *Pediastrum* in OM. The C_{29} ααα(20*R*) regular sterane are abundant in terrestrial plants (Grantham and Wakefield 1988). However, some studies have suggested that C_{29} ααα(20*R*) regular sterane is derived from *Cyanobacteria* or green algae (Berkaloff et al. 1983; Derenne et al. 1992) and possibly even from *Pediastrum* (Makeen et al. 2019). However, the relative content of C_{29} ααα(20*R*) regular sterane did not appear to be significantly related to that of *Pediastrum* (Figs. 9 and 10; Fig. 11b). It should be clarified that observations of maturity-related changes are based on artificially matured samples.

Paleoenvironment reconstruction

Paleoclimate

The OM enrichment was typically affected by paleoclimate which exerts a primary control on precipitation and therefore terrestrial OM input (Tanaka et al. 2007). In addition, paleoclimate changes affect terrigenous input and lake level

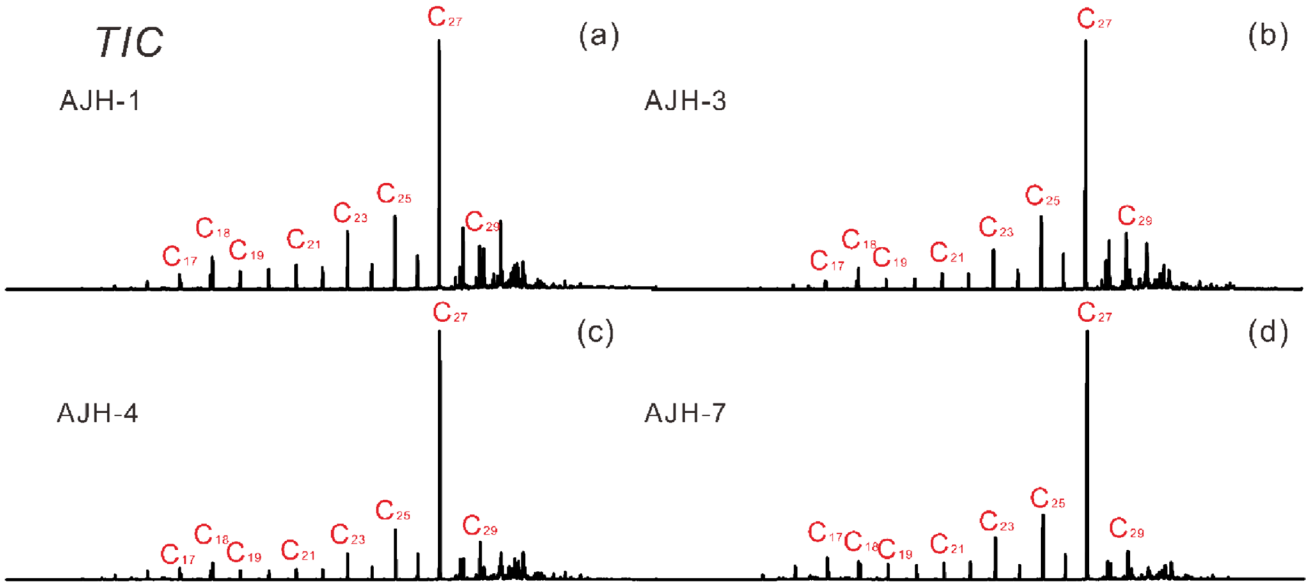

Fig. 7 Total ion current (TIC) fragmentograms of saturated fractions from the E_{2+3a} shale samples

Table 3 Aliphatic hydrocarbon of the E_{2+3a} shale samples, Junggar Basin

Samples	1	2	3	4	5	6	7	8	9	10	11
AJH-1	0.76	0.36	0.43	32.17	0.021	0.50	0.23	0.42	0.19	0.39	0.91
AJH-2	0.59	0.28	0.25	31.97	0.043	0.34	0.19	0.40	0.22	0.39	0.97
AJH-3	0.79	0.25	0.44	34.79	0.023	0.27	0.17	0.47	0.16	0.38	0.81
AJH-4	0.77	0.39	0.5	31.44	0.038	0.15	0.21	0.41	0.16	0.43	1.07
AJH-5	0.81	0.37	0.87	34.97	0.044	0.25	0.24	0.42	0.13	0.45	1.07
AJH-6	0.78	0.51	0.55	33.19	0.047	0.22	0.23	0.45	0.11	0.44	0.97
AJH-7	1.02	0.34	0.51	27.74	0.031	0.21	0.19	0.48	0.25	0.28	0.58
AJH-8	0.67	0.38	0.53	31.26	0.021	0.31	0.24	0.44	0.21	0.35	0.80

Note:1, Pr/Ph; 2, Pr/ *n*-C_{17}; 3, Ph/*n*-C_{18}; 4, *n*-C_{27} (%); 5, Ts/Tm; 6, Gammacerane/C_{30}hopane; 7, C_{30}mortane/ C_{30}hopane; 8, C_{27}ααα(20R) sterane/ (C_{27}ααα(20R) sterane + C_{28}ααα(20R) sterane + C_{29}ααα(20R) sterane); 9, C_{28}ααα(20R) sterane/ (C_{27}ααα(20R) sterane + C_{28}ααα(20R) sterane + C_{29}ααα(20R) sterane);10, C_{29}ααα(20R) sterane/ (C_{27}ααα(20R) sterane + C_{28}ααα(20R) sterane + C_{29}ααα(20R) sterane);11, C_{27}ααα(20R) sterane/ C_{29}ααα(20R) sterane

changes, which lead to changes in the chemical properties of lake basins, such as paleosalinity and redox conditions (Zhang et al. 2020). The distribution of trace elements deposited in sedimentary systems can be influenced by paleoenvironmental controls (Tribovillard et al. 2006). In arid climates, the Sr concentration increases, therefore, the Rb/Sr ratio decrease, while in humid climates, the Sr concentration decreases and resulting in increasing Rb/Sr ratio (Yandoka et al. 2015). Generally, a Sr/Cu ratio in the range of 1.3–5.0, 5–10, > 10 indicate a warm and humid climate, semi-humid to semi-arid climate, and a hot and arid climate, respectively (Lerman et al. 1978). Moreover, a lower Fe/Mn ratio commonly indicates a hot and arid paleoclimate (Lerman et al. 1978).

The Sr/Cu distribution of the E_{2+3a} shale was 4.76–15.25, with an average of 10.51 (Fig. 12a; Table 2), indicating that the E_{2+3a} depositional period was in a dry and hot climate, with a few periods being relatively warm and humid. The Rb/Sr ratios of the E_{2+3a} shale ranged 0.20–0.60 (Table 2), with an average of 0.34, which also indicated that the E_{2+3a} experienced hot and arid climate conditions as suggested by the variations in the Fe/Mn, Rb/Sr, and Sr/Cu ratios (Fig. 13c, d, and e, respectively). Stage "A" and Stage "B" of the E_{2+3a} had significant differences in the paleoenvironment, which in turn influenced the development of *Pediastrum*. Stage "A" of the E_{2+3a} was deposited under hot and arid climate conditions, while Stage "B" varied from hot and arid to warm and humid. Simultaneously, the TOC and *Pediastrum* contents and *n*-C_{27} fluctuated regularly following the paleoclimate changes (Fig. 13a, b, and q, respectively). This indicates that *Pediastrum* was relatively well developed in the Stage "B" depositional period, with high *n*-C_{27}, while

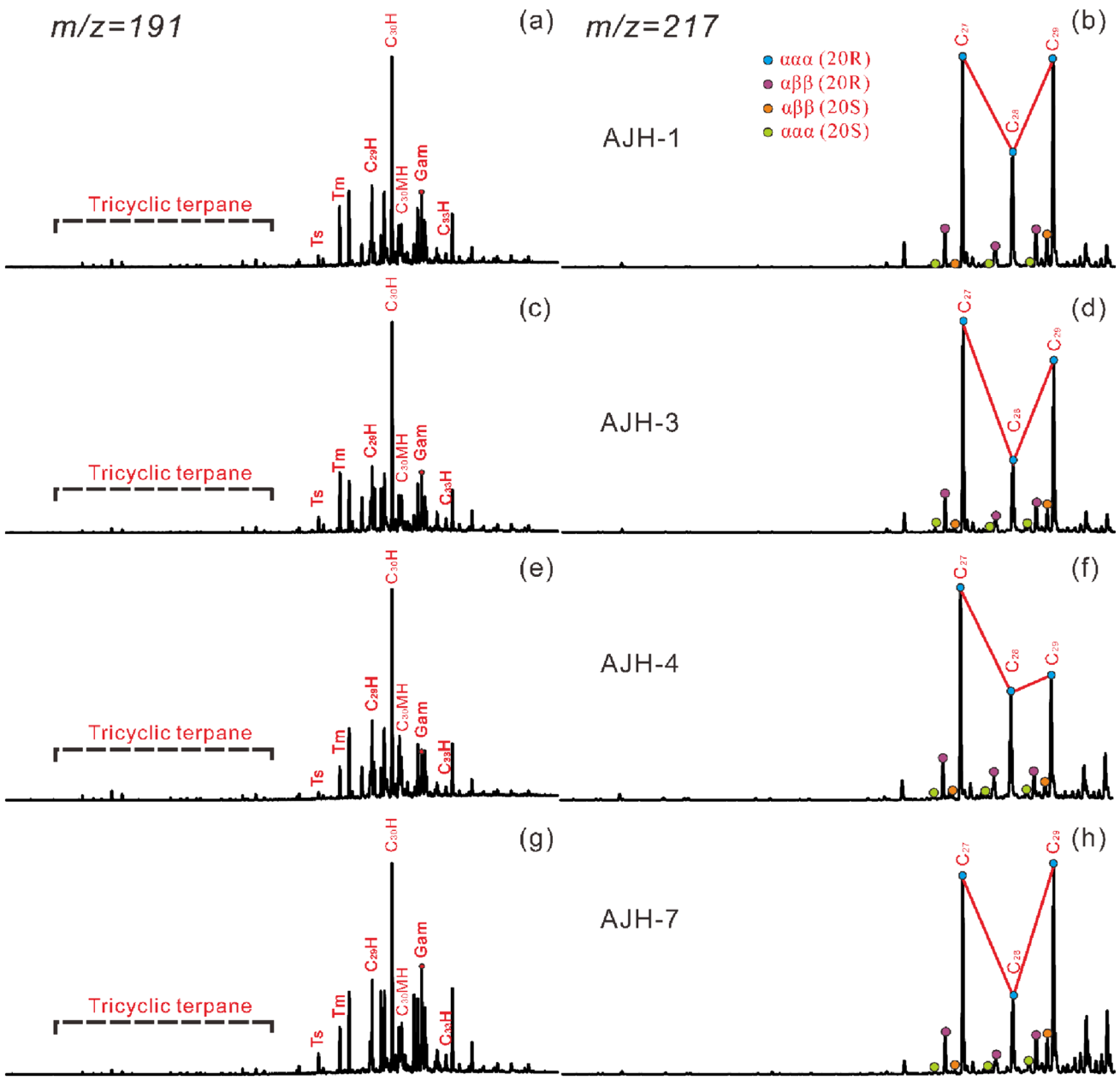

Fig. 8 Terpene (m/z 191) and sterane (m/z 217) fragmentograms of the E_{2+3a} shale samples

its content was relatively low in the Stage "A" depositional period, with a low *n*-C_{27}, which reflects that the paleoclimate during the E_{2+3a} sedimentation may have had a certain impact on *Pediastrum* accumulation.

Paleosalinity

Paleosalinity is vital for analyzing the paleo-sedimentary environment of lake basins (Liu et al. 2007; Fan et al. 2012) and has specific effects on OM preservation and biological growth (Wei et al. 2018). Different sedimentary microenvironments control the distributions and enrichments of different elements. Therefore, the sizes and distributions of the characteristic element ratios are also reasonably correlated with water salinity (Algeo and Maynard 2004). The Sr/Ba ratio is an empirical indicator of paleosalinity (Raiswell 1988; Makeen et al. 2019). When the soluble bicarbonate, chloride, and sulfate enter the lacustrine basin, the mobility of Ba becomes significantly lower than that of Sr as the solubility of Ba compounds is lower than that of Sr compounds and $BaSO_4$ precipitates easily (Hofer et al. 2013). As such, in the saline solution of the basin, the Sr content increases relatively with an increase in the offshore distance (Zheng et al. 1999; Chen et al. 2008). In general, a Sr/Ba

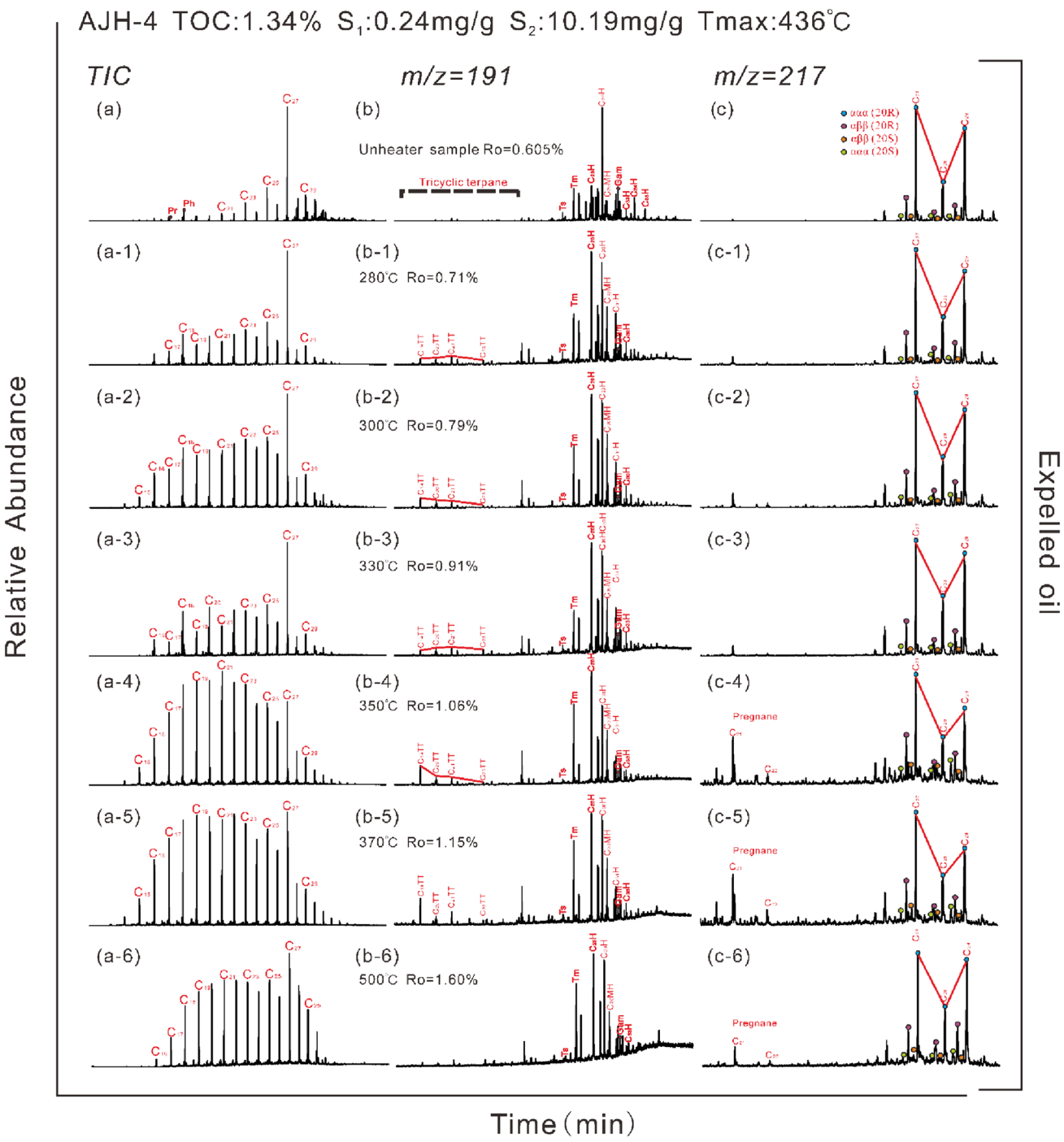

Fig. 9 TIC, terpene (m/z 191), and sterane (m/z 217) fragmentograms of the expelled oil

ratio greater than 1.0 indicates saline water, a Sr/Ba ratio 0.6–1.0 indicates brackish water, and a Sr/Ba ratio lower than 0.6 indicates freshwater (Zheng et al. 1999; Deng et al. 2018; Song et al. 2022). The Mo and TOC contents can also reflect the restrictiveness of lakes (Rowe et al. 2008). The Mo replenishment is affected in tightly restricted basins, and the Mo/TOC ratios in sediments are low (Huang et al. 2020). In addition, under dry climate conditions, the evaporation of lake water is greater than the water supply, the water level of the lake decreases, and the salinity of the water body increases relatively (Yandoka et al. 2015).

Gammacerane has become a standard component of OM and petroleum since Hills et al. (1966) identified it in the Green River oil shale in Colorado, USA. It is produced at the

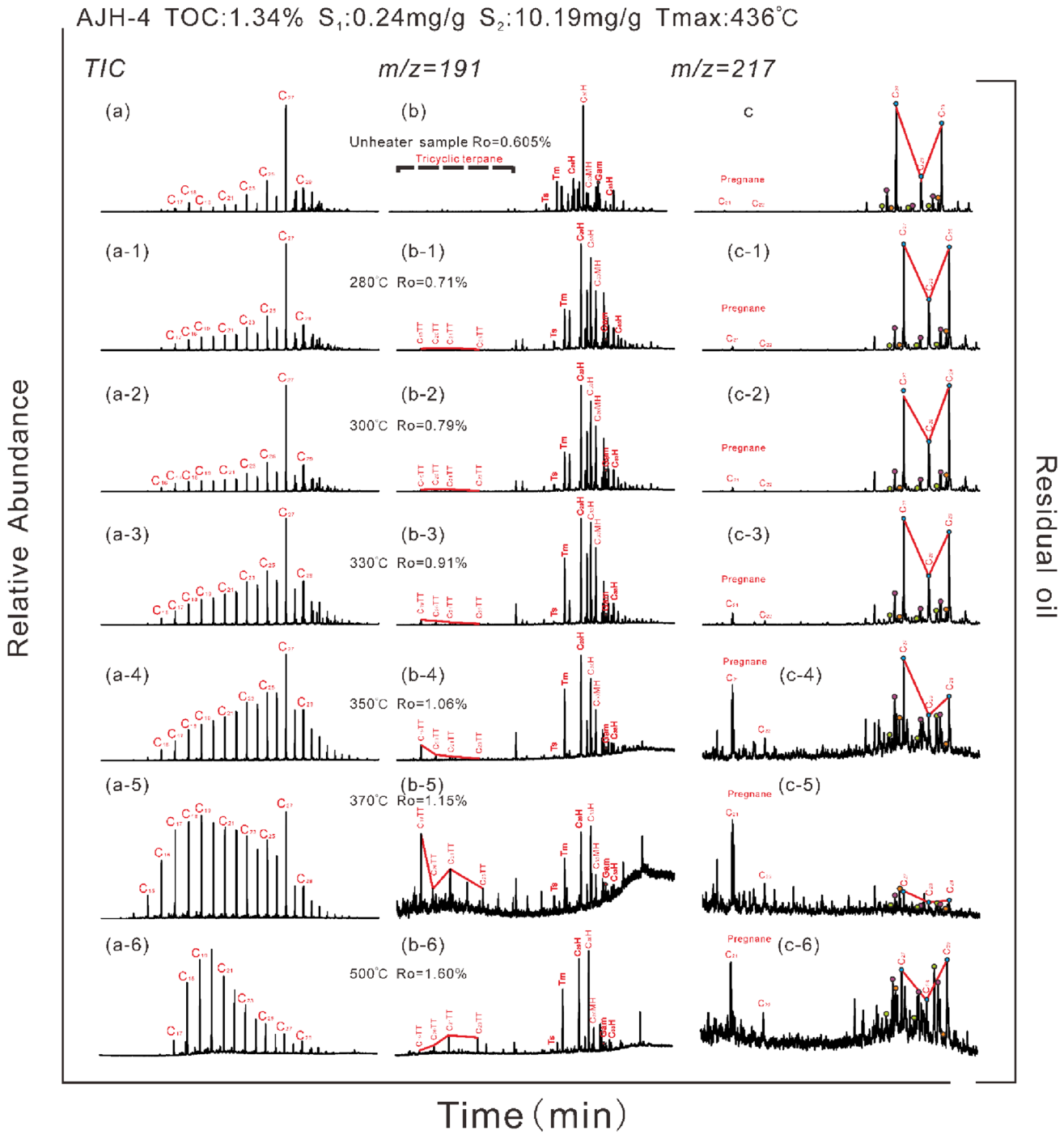

Fig. 10 TIC, terpene (m/z 191), and sterane (m/z 217) fragmentograms of the residual oil

chemocline by bacterivorous ciliates incorporating tetrahymonol and is generally considered to be a C_{30} pentacyclic triterpenoid produced during tetragonal diagenesis; a high abundance of gammacerane usually indicates high salinity in stratified water, a high G/C_{30}H ratio in OM indicates a high-salinity sedimentary environment (Moldowan et al. 1985). In addition, when the contribution of halophilic bacteria is high, a Pr/Ph ratio lower than 0.8 can be used to indicate high salinity waters (Peters et al. 2005). The salinization of lakes increases water density, forming relatively stable water column stratification conditions (Yandoka et al. 2015). Moreover, increasing water salinity reduces water infiltration and bioturbation, which are beneficial for OM preservation (Zheng et al. 1999; Chen et al. 2008).

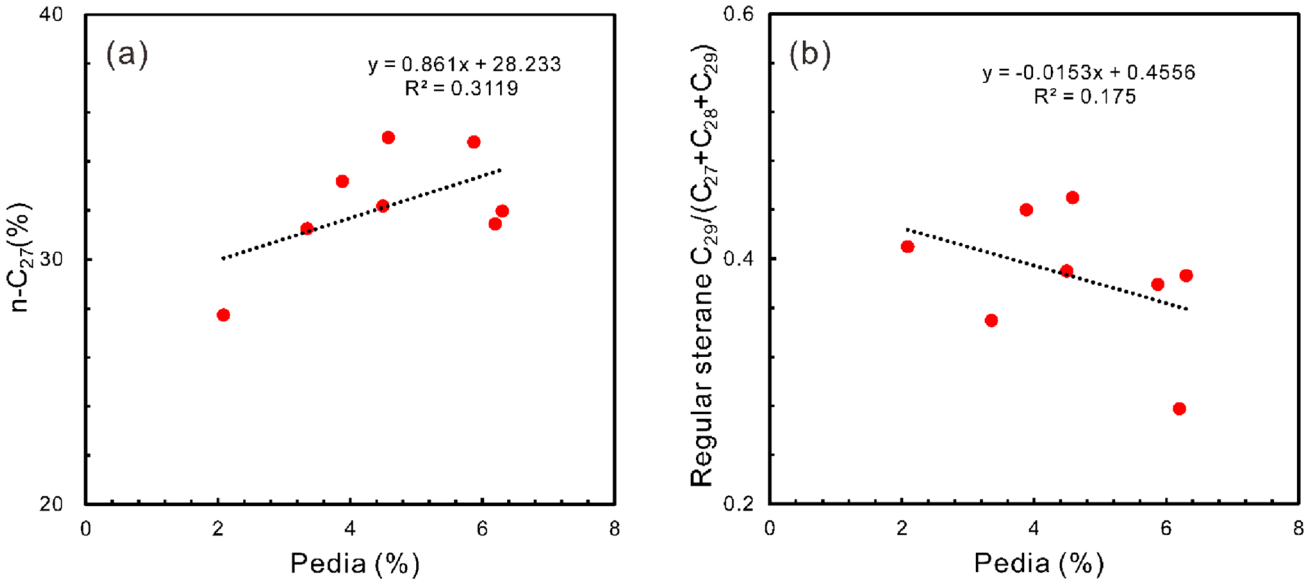

Fig. 11 **a** Cross plot of *n*-C_{27} versus the *Pediastrum* content; **b** Cross plot of regular sterane $C_{29}/(C_{27}+C_{28}+C_{29})$ versus the *Pediastrum* content. Abbreviations: Pedia, *Pediastrum*. Note: Regular sterane $C_{29}/(C_{27}+C_{28}+C_{29})$, C_{29}ααα(20*R*) sterane/(C_{27}ααα(20*R*) sterane + C_{28}ααα(20*R*) sterane + C_{29}ααα(20*R*) sterane). Note: *n*-C_{27}, abundance of *n*-C_{27} / abundances of saturated hydrocarbons

The Sr/Ba, G/C_{30}H, and Pr/Ph ratios of the E_{2+3a} shale (Fig. 13b, c, f, and h; Table 2 and 3) indicate that the shale was deposited in brackish to saltwater. The Mo/TOC ratios ranged 1.56–4.65 (avg. 3.12) (Figs. 12d and 13g; Table 2), i.e., they were lower than 4.5, thereby being close to the ratio for the Black Sea, formed in a strongly restrictive environment (Deng et al. 2018). The results showed that the paleosalinity in Stage "A" of E_{2+3a} was relatively high and that the sedimentary environment in Stage "B" was mainly brackish water, which is consistent with the results of the paleoclimate analysis (Fig. 13f, g, h, and i). This result also indicates that paleosalinity is closely related to paleoclimate conditions, hot and arid climate conditions and high salinity (Stage "A") are not conducive to *Pediastrum* development. Contrarily, a suitable climate and salinity (Stage "B") significantly increase the *Pediastrum* content (Fig. 13b and q).

Paleowater depth

In general, the water column stratification is easier to develop in deep-water bodies, and to form anoxic sedimentary environment is easier, which is more conducive to the preservation of OM (Rao and Huang 2017). Various elements exhibit different stabilities during sediment transportation (Wersin et al. 1991). Generally, Mn is more stable than Fe and Ti; thus, its transportation distance is relatively long (Wu et al. 2022). Typically, lower Mn/Ti and Mn/Fe ratios reflect shallow paleowater depths (Wersin et al. 1991). The Zr/Rb ratio can also be used to reflect paleowater depth (Dypvik and Harris 2001), and the Zr/Rb ratio decreases with increasing water depth.

The Mn/Ti, Mn/Fe, and Zr/Rb ratios in the E_{2+3a} shale were in the range of 0.10–0.17 (avg. 0.13), 0.010–0.018 (avg. 0.013), and 0.86–1.13 (avg. 0.99) (Table 2), respectively, indicating a decreased water depth during the depositional period, which reflects a shallow to semi-deep lake depositional environment. According to previous studies, the water depth for the development of *Pediastrum* generally does not exceed 15 m (Nielsen et al. 1992; Zhou et al. 2012). The results indicate that Stage "A" of the E_{2+3}a was generally deposited in a shallow water environment, while the water depth in Stage "B" was relatively deep during sedimentation (Fig. 13j, k, and m).

Redox conditions

Changes in redox conditions are generally related to water depth and lake turbulence, which are more critical for the preservation of OM than paleosalinity conditions (Bentum et al. 2012). The concentration of certain trace elements such as V, Cr, and Ni in sediments is closely related to the redox environment of the water during the depositional period (Self et al. 2006). In general, a V/ (V + Ni) ratio greater than 0.84 reflects stratification of the water column and results in anoxic bottom waters; a moderate V/ (V + Ni) ratio, between 0.54 and 0.72, indicates an anoxic environment with weak water column stratification. The parameter δU is commonly used for analyzing Redox conditions. A δU ratio (δU = 2U/ (U + Th/3) greater than 1.0 indicates an

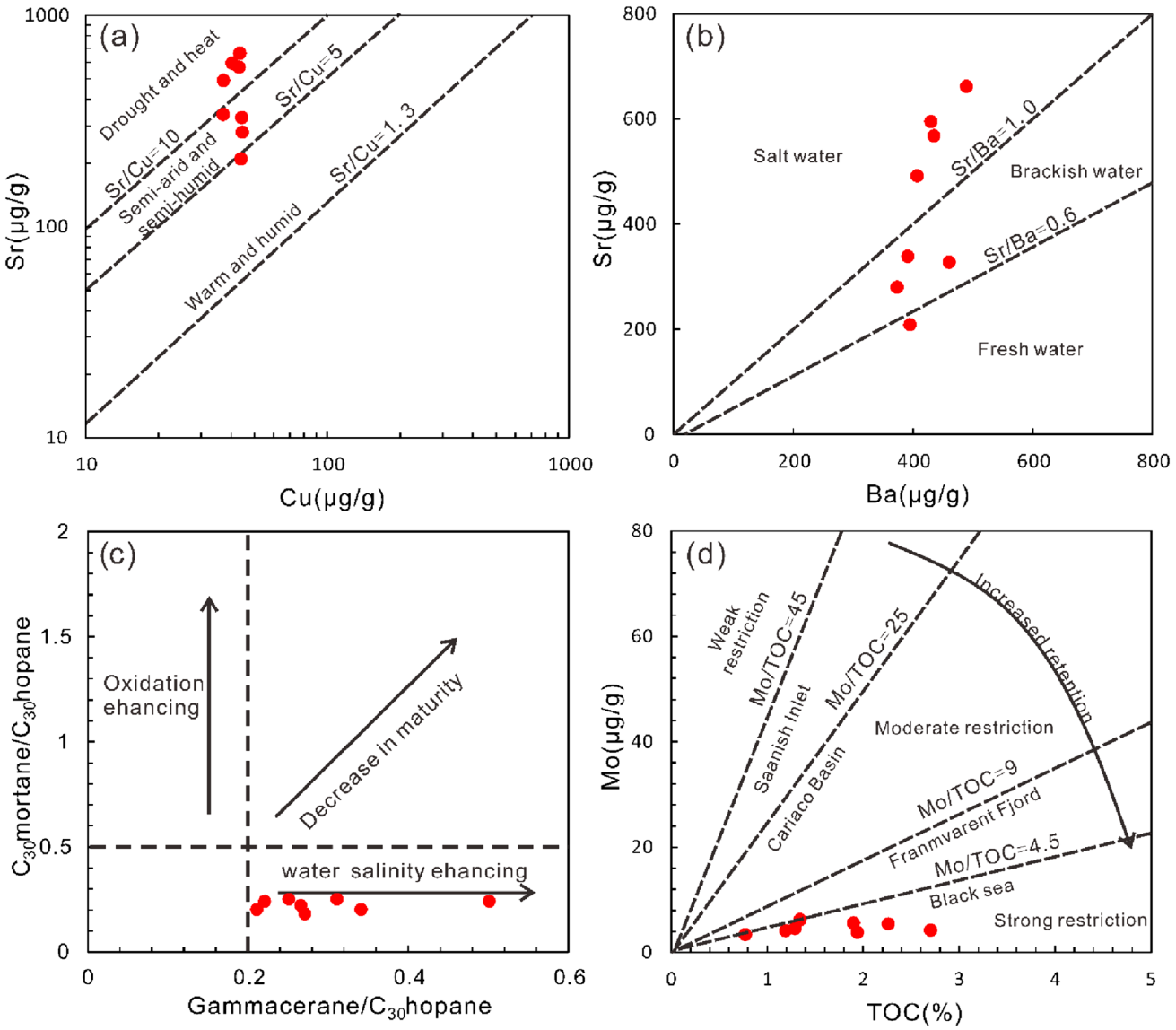

Fig. 12 **a** Cross plot of Sr versus Cu representing the paleoclimate of the sedimentary period of the E_{2+3a}. **b** Cross plot of Sr versus Ba representing water salinity during the sedimentary period of the E_{2+3a}. **c** Cross plot of C_{30}mortane/C_{30}hopane versus Gammacerane/C_{30}hopane characterizing water salinity, redox conditions, and maturity of the E_{2+3a}. **d** Cross plot of Mo versus TOC representing water closure during sedimentation of the E_{2+3a}

anoxic environment, whereas, a δU lower than 1.0 suggests an oxidation environment (Wignall and Myers 1988; Steiner et al. 2001; Algeo and Maynard 2004). A low Mn/Fe ratio also indicates anoxia in the water body (Kuma et al. 2019). The Pr/Ph ratios of < 0.5, 0.5–1.0, 1.0–3.0, and > 3.0 correspond to anoxic, reducing, weakly reducing to weakly oxidizing, and oxidizing conditions, respectively (Mei and Liu, 1980; Mello et al., 1988). Additionally, lower Pr/*n*-C_{17} and Ph/*n*-C_{18} ratios generally suggest a reducing environment, providing key insights into the depositional conditions of organic matter.

The V/ (V + Ni) and δU ratios of the E_{2+3a} shale ranged 0.60–0.68 (avg. 0.64) and 0.86–1.29 (avg. 1.03), respectively (Table 2), indicating a reducing environment, this was corroborated by the Pr/Ph, Pr/*n*-C_{17}, and Ph/*n*-C_{18} ratios (Table 3). Therefore, we can confirm that the E_{2+3a} shale was deposited during anoxic conditions which were favorable for preventing scavenging of OM. The results showed that the preservation condition of Stage "A" of the E_{2+3a} was slightly better than that of Stage "B", which may be related to the water turbulence caused by terrigenous input during the depositional period of Stage "B" (Fig. 13n and o) (Table 4).

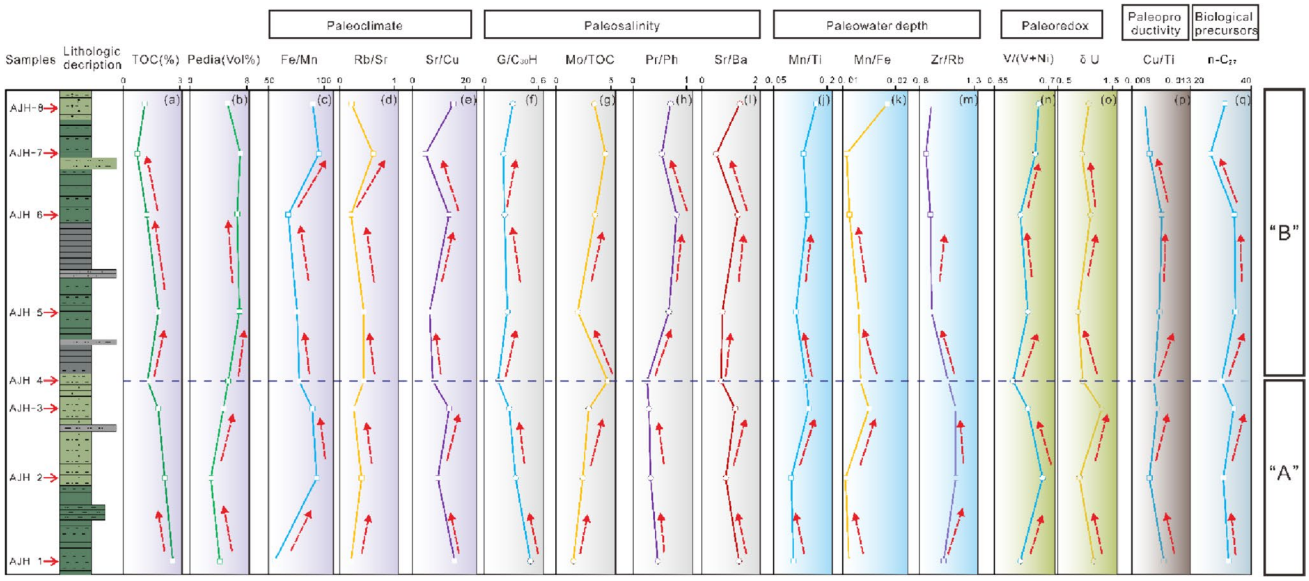

Fig. 13 Variations of paleoclimate, paleosalinity, paleowater depth, paleoredox, and paleoproductivity of the samples from E_{2+3a}

Table 4 Aliphatic hydrocarbon of the hydrous pyrolysis products of the E_{2+3a} shale

Unheated sample	Temperature (℃)	Ro (%)	Liquid hydrocarbon	1	2	3	4	5
AJH-4	280	0.71	Expelled oil	0.11	0.08	1.11	0.36	0.45
	300	0.79		0.08	0.03	1.06	0.37	0.44
	330	0.91		0.16	0.11	1.09	0.37	0.42
	350	1.06		0.10	0.03	1.43	0.32	0.48
	370	1.15		0.12	0.06	1.02	0.32	0.47
	500	1.60		0.20	0.11	1.07	0.39	0.41
	280	0.71	Residual oil	0.10	0.02	1.16	0.40	0.41
	300	0.79		0.21	0.02	1.17	0.42	0.38
	330	0.91		0.08	0.02	1.04	0.38	0.43
	350	1.06		0.10	0.04	1.32	0.31	0.50
	370	1.15		0.21	0.21	0.95	0.30	0.45
	500	1.60		0.08	0.16	0.92	0.45	0.34

Note: 1, Gammacerane/C_{30}hopane; 2, Ts/ Tm; 3, C_{29}hopane / C_{30}hopane; 4, C_{29}ααα(20R) sterane/ (C_{27}ααα(20R) sterane + C_{28}ααα(20R) sterane + C_{29}ααα(20R) sterane);5, C_{27}ααα(20R) sterane/ (C_{27}ααα(20R) sterane + C_{28}ααα(20R) sterane + C_{29}ααα(20R) sterane)

Paleoproductivity

Generally, the Cu enrichment rate in lake sediments is closely related to productivity (Holland 1978; Wan et al. 2003). Therefore, the Cu/Ti ratio is considered to be an effective indicator for the reconstruction of primary productivity, and in general, higher Cu/Ti ratios indicate higher paleoproductivity (Shen et al. 2015).

The Cu/Ti ratio of the E_{2+3a} shale ranged 0.009–0.011 (avg. 0.010) (Table 1), which was higher than that of the Post-Archean Australian shale (PAAS) with average Cu/Ti ratio 0.008, indicating that the E_{2+3a} shale had increased paleoproductivity. In addition, a good correlation was observed between the relative content of *Pediastrum* and the Cu/Ti ratio (Fig. 13p and q). The results showed that the paleoproductivity of Stage "A" of E_{2+3a} was lower than that of Stage "B," which may be attributed to the *Pediastrum* development.

OM formation model

During the deposition of the E_{2+3a} shale, the water depth changed frequently while being generally shallow, the climate was hot and arid, evaporation was intense, and water salinity was high. Paleoclimate affects the salinity, depth, and redox conditions of water by controlling evaporation.

Conditions during the deposition of the E_{2+3a} shale are conducive to OM preservation, and the abundance and type of OM are mainly controlled by water salinity (Makeen et al. 2015). However, the abundance of OM does not increase with salinity; "salinity critical points" exist for different organisms and when salinity exceeds these critical points, the number of organisms plummets (Hu et al. 2021). *Pediastrum* also exhibits a "salinity critical point" beyond which increased salinity negatively impacts its growth. However, due to the limited number of data points available, this tipping point requires further refinement and investigation. Carbonate minerals are considered suitable carriers of paleoclimate information in lake sediments because of their wide spatiotemporal distributions as well as their sensitive responses to environmental changes (Gao et al. 2018). For semi-closed to closed lakes in arid to semi-arid areas, an increase in lake evaporation can promote carbonate deposition. For example, Selin Co is a closed lake on the Qinghai–Tibet Plateau, and the variation of carbonate mineral content in the lake is negatively correlated with precipitation intensity. Therefore, more carbonate minerals in the sediments indicate higher salinity (Kaufman et al. 1991). XRD and rock thin-section analyses showed that the E_{2+3a} shale was mainly composed of clay, felsic, and carbonate (dolomite and calcite) minerals (Table 1). With an increase in the carbonate mineral content, the *Pediastrum* content first increased and then decreased (Fig. 14a). Additionally, n-C_{27} versus the G/ C_{30}H ratio and *Pediastrum* versus the G/ C_{30}H ratio showed similar trends (Fig. 14b and c, respectively). This means that the *Pediastrum* content increases and then decreases as salinity increases, and this "salinity critical point" corresponds to an approximate G/C_{30}H ratio of 0.34 (Fig. 14b and c). These results contrast with those of previous studies suggesting *Pediastrum* is a freshwater alga with poor salt tolerance (Xiao et al. 1996; Zamaloa and Tell 2005; Wan et al. 2008; Brenner et al. 2006).

The paleoclimate of Stage "A" was relatively hot and arid, with water depth reduced, the input of terrestrial OM reduced, and the high evaporation of the water; all these resulted in high salinity in the water and a reduction of the *Pediastrum* content (Fig. 15a). Stage "B" of the E_{2+3a} deposition was warm and humid, and rivers brought a large amount of freshwater and terrigenous OM into the lake, leading to an increase in felsic minerals and a relative decrease in carbonate minerals. At the same time, water salinity decreased, resulting in a relatively high abundance of *Pediastrum* (Fig. 15).

Conclusion

(1) The E_{2+3a} shale displays a notable abundance of OM, predominantly characterized by Type I and II kerogens, with a lesser presence of Type III OM, indicating a more favorable oil-generating potential.

(2) *Pediastrum* emerges as the predominant OM contributor to hydrocarbon generation in the E_{2+3a} shale, with its relative content exhibiting a positive correlation with TOC. Moreover, the presence of n-C_{27} may serve as a distinctive biomarker indicative of *Pediastrum*.

(3) Throughout the depositional period of the E_{2+3a} shale, the climate was characterized by hot and arid conditions, accompanied by an increase in salinity. These environmental factors created optimal conditions for the preservation of organic matter within the shale. Moreover, the conducive salinity environment likely facilitated the proliferation of *Pediastrum* during this period, and the "salinity critical point" for Pediastrum may be identified at G/C_{30}H = 0.34.

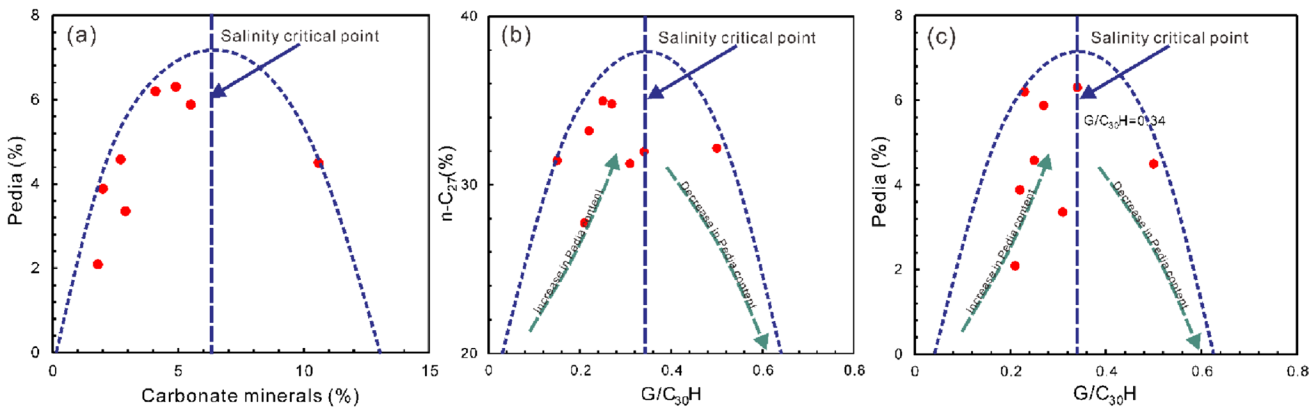

Fig. 14 **a** Cross plot of the carbonate content versus the *Pediastrum* content. **b** Cross plot of the Gammacerane/C_{30}hopane content versus the n-C_{27} ratio. **c** Cross plot of the Gammacerane/C_{30}hopane content versus the *Pediastrum* content. Abbreviations: Pedia, *Pediastrum*

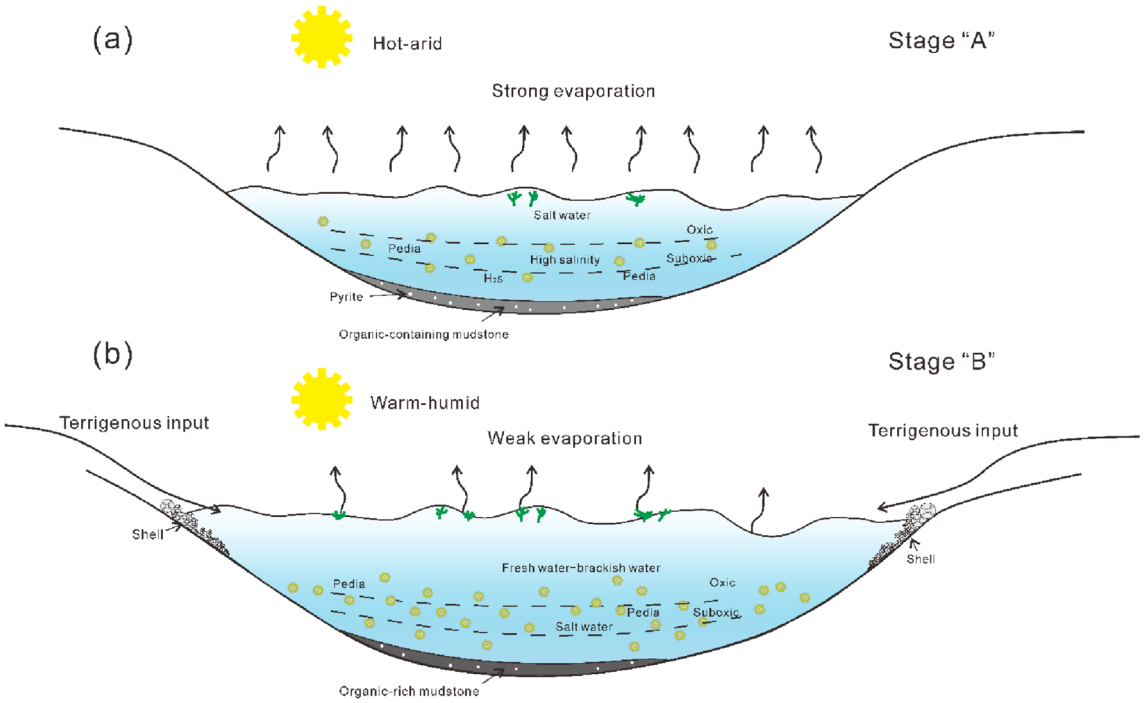

Fig. 15 OM enrichment models of the E_{2+3a} shale in the Junggar Basin. **a** In the early deposition, the area was an enclosed basin with a restricted water condition. **b** In the late sedimentary period, terrigenous input increased

Supplementary Information The online version contains supplementary material available at https://doi.org/10.1007/s00531-024-02415-9.

Acknowledgements Thank you to Xinjiang Oilfield Company for funding this research (2020-C4006), and also thank to China University of Petroleum (Beijing) for the advanced experimental equipment. Thanks to the anonymous reviewers and editors for their comments, which greatly improved the quality of the manuscript.

Funding Xinjiang Oilfield Company, 2020-C4006, Gang Gao.

Data availability The data that support the findings of this study are available. If you have any questions about accessing the data or need further information on the data usage restrictions, please contact gg_2819@163.com.

Declarations

Conflict of interest We declare that we have no financial and personal relationships with other people or organizations that can inappropriately influence our work, there is no professional or other personal interest of any nature or kind in any product, service and/or company that could be construed as influencing the position presented in, or the review of, the manuscript entitled "***Sedimentary environment and a development model for source rocks rich in the green alga Pediastrum: A case study of the Paleogene Anjihaihe Formation in the Junggar Basin, Northwest China***".

References

Algeo TJ, Maynard JB (2004) Trace-element behavior and redox facies in core shales of upper pennsylvanian kansas-type cyclothems. Chem Geol 206(3–4):289–318. https://doi.org/10.1016/j.chemgeo.2003.12.009

Bai H, Pang XQ, Kuang LC, Pang H, Pang Y, Zhou LM (2016) Formation conditions of deep hydrocarbon in junggar basin, NW China. Petrol Geol. & Exp 38(06):803–810. https://doi.org/10.13745/j.esf.sf.2019.1.12

Bentum EVC, Reichart GJ, Sinninghe-Damst JS (2012) Organic matter provenance, palaeoproductivity and bottom water anoxia during the cenomanian/turonian oceanic anoxic event in the newfoundland basin (northern proto north atlantic ocean). Org Geochem 50:11–18. https://doi.org/10.1016/j.orggeochem.2012.05.013

Berkaloff C, Casadevall E, Largeau C (1983) The resistant polymer of the walls of the hydrocarbon-rich alga botryococcus braunii. Phytochem 22(2):389–397. https://doi.org/10.1016/0031-9422(83)83010-6

Brenner M, Hodell DA, Leyden BW, Curtis JH, Kenney WF, Gu BH, Newman JM (2006) Mechanisms for organic matter and phosphorus burial in sediments of a shallow, subtrop ical, macrophyte-dominated lake. J Paleolimnol 35:129–148. https://doi.org/10.1007/s10933-005-7881-0

Brocks P, Rohjans D, Scholz-Bottcher BM, Rullkotter J (1999) Molecular composition of organic matter in the sediment of a mussel

bee as an indicator of ecological variations. Mar Biodivers 29(5 Suppl):45–50. https://doi.org/10.1007/BF03043119
Chen ZH, Zha M, Jin Q (2008) Mineral elemental response to the evolution of terrestrial brine faulted-basin: a case study in the paleogene of well halke-1. Dongying Sag Acta Sedimentologica Sinica 26(06):925–932. https://doi.org/10.1103/PHYSREVLETT.102.175002
Chen JP, Wang XL, Ni YY, Xiang BL, Liao FR, Liao JD, Zhao CY (2019) Genetic type and source of nature gas in the southern margin of junggar basin, NW China. Pet Explor Dev 46(03):461–473
Demaison GJ, Moore GT (1980) Anoxic Environments and Oil Source Bed Genesis. Bull 64.
Deng X, Kang ZH, Peng YY, Xiao HF, Han HY, Yu XD (2018) element characteristics of shale in wufeng formation in southern sichuan basin indicating significance of paleo-tectonic and paleoenvironment. Coal Technol 37(05). https://doi.org/10.13301/j.cnki.ct.2018.05.050
Derenne S, Largeau C, Berkaloff C, Rousseau B, Wilhelm C, Hatcher PG (1992) Non-hydrolysable macromolecular constituents from outer walls of chlorella fusca and nanochlorum eucaryotum. Phytochem 31(6):1923–1929. https://doi.org/10.1016/0031-9422(92)80335-C
Doner Z, Kumral M, Demirel IH, Hu Q (2019) Geochemical characteristics of the Silurian shales from the central taurides, southern Turkey: organic matter accumulation, preservation and depositional environment modeling. Mar Pet Geol 102:155–175. https://doi.org/10.1016/j.marpetgeo.2018.12.042
Dypvik H, Harris NB (2001) Geochemical facies analysis of fine-grained siliciclastics using Th/U, Zr/Rb and (Zr+Rb)/Sr ratios. Chem Geol 181:131–146. https://doi.org/10.1016/S0009-2541(01)00278-9
Fan YH, Qu HJ, Wang H, Yang XC, Feng YW (2012) The application of trace elements analysis to identifying sedimentary media environment: a case study of late triassic strta in the middle part of western ordos basin. Geol Chin 39(02):382–389. https://doi.org/10.1016/j.still.2012.05.017
Gao G, Yang SR, Ren JL, Zhang W, Xiang BL (2018) Geochemistry and depositional conditions of the carbonate-bearing lacustrine source rocks: a case study from the early permian fengcheng formation of well FN7 in the northwestern junggar basin. J Petrol Sci Eng 162:407–418. https://doi.org/10.1016/j.petrol.2017.12.065
GB/T 14506.30-2010 (2010) Methods for chemical analysis of silicate rocks. Beijing, Standards Press of China.
Geel VB (2001) Non-pollen palynomorphs. In: Smol JP, Birks HJB, Last WM (eds) Tracking environmental change using lake sediments: terrestrial, algal, and siliceous indicators, vol 3. Kluwer, Dordrecht, pp 99–119. https://doi.org/10.1111/j.1365-2427.2004.01211.x
Geel VB, Odgaard BV, Ralska-Jasiewiczowa M (1996) Cyanobacteria as indicators of phosphate–eutrophication of lakes and pools in the past. Pact 50 IV. 5:399–415
Gosling WD, Mayle FE, Tate NJ, Killeen TJ (2009) Differen tiation between Neotropical rainforest, dry forest, and savannah ecosystems by their modern pollen spectra and implications for the fossil pollen record. Rev Palaeobot Palynol 153:70–85. https://doi.org/10.1016/j.revpalbo.2008.06.007
Grantham PJ, Wakefield LL (1988) Variations in the sterane carbon number distributions of marine source rock derived crude oils through geological time. Org Geochem 12:61–73. https://doi.org/10.1016/0146-6380(88)90115-5
He WJ, Fei LY, Yiming A, Yang HB, Lan WF, Ding J, Bao HJ, Guo WJ (2019) Accumulation conditions of deep hydrocarbon and exploration potential analysis in junggar basin NW China. Earth Sci Front 26(01):189–201. https://doi.org/10.13745/j.esf.sf.2019.1.12
Hills IR, Whitehead EV, Anders DE, Cummins JJ, Robinson WE (1966) An optically active triterpane, gammacerane, in Green River, Colorado, oil shale bitumen. J Chem Soc Chem Commun 20:752e754
Hofer G, Wagreich M, Neububer S (2013) 2013 Geochemistry of fine-grained sediments of the upper cretaceous to paleogene gosau group (Austria, Slovakia): implications for paleoenvironmental and provenance studies. Geosci Front 4(4):449–468. https://doi.org/10.1016/j.gsf.2012.11.009
Holland HD (1978) The chemistry of the atmosphere and oceans. Wiley-Interscience, New York (**10.1525/aa.1954.56.6.02a00260**)
Hu T, Pang XQ, Jiang FJ, Wang QF, Xu TW, Wu GY, Cai Z, Yu JW (2021) Factors controlling differential enrichment of organic matter in saline lacustrine rift basin: a case study of third member shahejie fm in dongpu depression. Acta Sedimentol Sin 39(01):140–152
Huang ZQ, Fang CG, Li JQ, Zhang CC, Wang YJ, Liu LX, Zhao S (2020) U-Mo covariance model of Wufeng-Gaojiabian Formation marine shale in Ningjing-Zhenjiang area and its implication for water retention degree in ancient sea basin. J Chengdu Univ Technol Sci Technol Ed 47(04):443–450
Komarek JaJV (2001) Review of the Green Algal Genus Pediastrum; Implication for Pollen-analytical Research. Bibl. Phycol.
Jiang WY, Guo ZT, Sun XJ (2006) Reconstruction of climate and vegetation changes of lake bayanchagan (inner mongolia): holocene variability of the east asian monsoon. Quat Res 65:411–420
Jiang QF, Ji JF, Shen J, Matsumoto RYO, Tong GB, Qian P, Ren XM, Yan DZ (2013) Holocene vegetational and climatic variation in westerly-dominated areas of central asia inferred from the sayram lake in northern Xinjiang. China Sci Sin (terrae) 43(02):243–255
Kaufman AJ, Hayes JM, Knoll AH, Germs GJB (1991) Isotopic compositions of carbonates and organic carbon from upper Proterozoic successions in Namibia, stratigraphic variation and the effects of diagenesis and metamorphism. Precambrian Res 49:301–327. https://doi.org/10.1016/0301-9268(91)90039-D
Kirellos J, Sefein AB, Thanh X, Nguyen AC, Philp RP (2017) Organic geochemical and paleoenvironmental characterization of the brown shale formation, kiliran sub-basin, central sumatra basin. Indonesia Org Geochem 112(2017):137–157. https://doi.org/10.1016/j.orggeochem.2017.06.017
Kristen I, Wilkes H, Vieth A, Zink KG, Plessen B, Thorpe J, Partridge TC, Oberhänsli H (2010) Biomarker and stable carbon isotope analyses of sedimentary organic matter from lake tswaing: evidence for deglacial wetness and early holocene drought from south africa. J Paleolimnol 44:143–160. https://doi.org/10.1007/s10933-009-9393-9
Krzeszowska E (2019) Geochemistry of the Lublin Formation from the Lublin coal basin: implication for weathering intensity, palaeoclimate and provenance. Int J Coal Geol 216(1):1–12. https://doi.org/10.1016/j.coal.2019.103306
Kuma R, Hasegawa H, Yamamoto K, Yoshida H, Ikeda M (2019) Biogenically induced bedded chert formation in the alkaline palaeolake of the green river formation. Sci Rep 9(1):16448. https://doi.org/10.1038/s41598-019-52862-7
Lamb H, Roberts N, Leng M, Barker P, Benkaddour A, van der Kaars S (1999) Lake evolution in a semi-arid montane environment: response to catchment change and hydrocli matic variation. J Paleolimnol 21:325–343. https://doi.org/10.1023/A:1008099602205
Lerman A, Baccini P (1978) Lakes: Chem Geol Phys. Springer—Verlag, New York
Liao J, Feng Q, Lu H, Sheng GY, Peng PA, Samuel HC (2022) n-C_{27} Predominance and ^{13}C enrichment by bicarbonate assimilation of race A of Botryococcus braunii in Chinese Maoming oilshales. Chem Geol 602:120905. https://doi.org/10.1016/j.chemgeo.2022.120905
Liu G, Zhou DS (2007) Application of Microelements analysis in identifying sedimentary environment-Taking Qianjiang Formation in

the Jianghan Basin as an example. Pet Geol Exp 03:307–310+314. https://doi.org/10.1016/S1872-5813(07)60034-6

Liu W, Yang H, Wang HY, Yao Y, Wang Z, Cao YN (2016) Influence of aquatic plants on the hydrogen isotope composition of sedimentary long-chain n-alkanes in the Lake Qinghai region. Qinghai-Tibet Plateau Sci China Earth Sci 59:1368–1377. https://doi.org/10.1007/s11430-016-5263-2

Liu B, Bechtel A, Gross D, Fu XF, Li XN, Sachsenhofer RF (2018) Middle Permian environmental changes and shale oil potential evidenced by high-resolution organic petrology, geochemistry and mineral composition of the sediments in the Santanghu Basin. Northwest China. Int. J. Coal Geol 185:119–137. https://doi.org/10.1016/j.coal.2017.11.015

Ma J, Wu CD, Wang YZ, Jiao Y, Zhou JQ, Leng JX, Cui XQ (2020) Discovery of carotenoids and paleolake significance in the oil-gocene anjihaihe formation, southern junggar basin China. Acta Geol Sin 94(06):1853–1868. https://doi.org/10.19762/j.cnki.dizhixuebao.2020075

Makeen YM, Hakimi MH, Abdullah WH (2015) The origin, type and preservation of organic matter of the Barremian-Aptian organic-rich shales in the Muglad Basin, Southern Sudan, and their relation to paleoenvironmental and paleoclimate conditions. Mar Pet Geol 65:187–197. https://doi.org/10.1016/j.marpetgeo.2015.03.003

Makeen YM, Abdullah WH, Ayinla HA, Shan X, Liang Y, Su S (2019) Organic geochemical characteristics and depositional setting of paleogene oil shale, mudstone and sandstone from onshore penyu basin, chenor, pahang, malaysia. Int J Coal Geol. https://doi.org/10.1016/j.coal.2019.03.012

Moldowan JM, Seifert WK, Gallegos EJ (1985) Relationship between petroleum composition and depositional environment of petroleum source rocks. AAPG Bull 69:1255–1268

Mukhopadhyay PK, Wade JA, Kruge MA (1995) Organic facies and maturation of Cretaceous/Jurassic rocks and possible oil-source rock correlation based on pyrolysis of asphaltenes, Scotian basin. Canada Org Geochem 22:85–104. https://doi.org/10.1016/0146-6380(95)90010-1

Nielsen H, Sørensen I (1992) Taxonomy and stratigraphy of late glacial Pediastrum taxa from Lysmosen, Denmark – a preliminary study. Rev Palaeobot Palynol 74:55–75. https://doi.org/10.1016/0034-6667(92)90138-7

Pan YS, Huang ZL, Li TJ, Guo XB, Chen X (2020) Environmental response to volcanic activity and its effect on organic matter enrichment in the permian lucaogou formation of the malang sag, santanghu basin, northwest china. Palaeogeogr Palaeocl 560(11):110024. https://doi.org/10.1016/j.palaeo.2020.110024

Peters KE, Cassa MR (1994) Applied source rock geochemistry. In: Magoon LB, Dow WG (eds) The Petroleum System – from Source to Trap. AAPG Tulsa, OK, pp 3–117

Peters KE, Walters CC, Moldowan JM (2005) The Biomarker Guide: Biomarkers and Isotopes in Petroleum Exploration and Earth History, 2nd edn. CUP, Cambridge, p 2

Qin JZ, Li ZM, Liu BQ, Zhang Q (2007) The potential of generating heavy oil and solid bitumen of excellent marine source rocks. Pet Geol Exp 03:280–285+291

Qin J, Lin XY, Pan H, He B (2014) Correlations between the sikeshu sag and the oil source rock in its peripheral region, south junggar basin. Bull Mineral Petrology Geochem 33(03):395–400

Raiswell RF, Buckley BRA (1988) Degree of pyritization of iron as a paleoenvironmental indicator of bottom-water oxygenation. J Sediment Res 58:812–819

Rao HM, Huang WG (2017) Discussion on influencing factor of content of dissolved oxygen in water. J Salt Sci Chem Ind 46(3):40–43

Riboulleau A, Schnyder J, Riquier L, Lefebvre V, Deconinck J-F (2007) Environmental change during the early cretaceous in the purbeck-type durlston bay section (dorset, southern england): a biomarker approach. Org Geochem 38:1804–1823. https://doi.org/10.1016/j.orggeochem.2007.07.006

Rowe HD, Loucks RG, Ruppel SC, Rimmer SM (2008) Mississippian barnett formation, fort worth basin, texas: bulk geochemical inferences and Mo–TOC constraints on the severity of hydrographic restriction. Chem Geol 257:16–25. https://doi.org/10.1016/j.chemgeo.2008.08.006

Self S, Widdowson M, Thordarson T, Jay AE (2006) Volatile fluxes during flood basalt eruptions and potential effects on the global environment: a deccan perspective. Earth Planet Sci Lett 248(1–2):518–532. https://doi.org/10.1016/j.epsl.2006.05.041

Shen J, Schoepfer SD, Feng QL, Zhou L, Algeo TJ (2015) Marine productivity changes during the permian-triassic boundary crisis and early triassic recovery.

Sherwood N (1991) Oil shales. PhD Thesis Volume 1 and Volume 2. University of Wollongong.

Song G, Miao ZY, Du SR, Li XM (2022) Geochemical characteristics of trace elements before and after the upper salt forming perid of the MK-3 core, simao basin and their paleoenvirnonment implications. Acta Geosci Sin, 1–9.

Song YT, Li SQ (1995) Thermal simulation experimental study on hydrocarbon generation by coccolithophores. Geol J China Univ 02:95–106

Stach EM, Mackowsky MTH, Teichmüller M, Taylor GH, Teichmüller R (1982) Stach's text book of coal petrology, 3rd edn. Gebruder Bomtraeger, Berlin, pp 87–140

Stein BB (2009) Black shale formation in the late paleocene/early eocene arctic ocean and paleoenvironmental conditions: new results from a detailed organic petrological study. Mar Pet Geol. https://doi.org/10.1016/j.marpetgeo.2008.04.001

Steiner M, Wallis E, Erdtmann BD, Zhao YL, Yang RD (2001) Submarine – hydrothermal exhalative ore layers in black shales from South China and associated fossils – insights into a lower Cambrian facies and bio-evolution. Palaeogeogr Palaeocl 169:165–191. https://doi.org/10.1016/S0031-0182(01)00208-5

Sun XJ, Wu YS (1987) Distribution and quantitative characteristics of pollen and algae in surface sediments of dianchi lake. Yunnan Mar Geol Quat Geol 04:81–92. https://doi.org/10.1016/S0034-6667(98)80011-0

Sylvestre F (2002) A high-resolution diatom reconstruction between 21,000 and 17,400 14C yr BP from the southern bolivian altiplano (18–23 S). J Paleolimnol 27:45–57. https://doi.org/10.1023/A:1013542907394

Tanaka K, Akagawa F, Yamamoto K, Tani Y, Kawabe I, Kawai T (2007) Rare earth element geochemistry of Lake Baikal sediment: its implication for geochemical response to climate change during the last Glacial/Interglacial transition. Quat Sci Rev 26:1362–1368. https://doi.org/10.1016/j.quascirev.2007.02.004

Tang Y, Song Y, Guo XG, Zhao JZ, Wu T, Huang LL, He WJ, Wu WT, Wu HY (2022) Main controlling factors of tight conglomerate oil enrichment above source kitchen in mahu sag junggar basin. Acta Petrol Sin 43(02):192–206

Tian AQ, Chen S, Yu YX, Xiu JL, Jin F (2022) Layered deformation characteristics, formation mechanism strike slip faults on the western edge of mosuowan uplift. Geosci 1–15. https://doi.org/10.19657/j.geoscience.1000-8527.2022.035

Tissot BP, Welte DH (1984) Petroleum formation and occurrence. Springer Verlag, Berlin Heidellberg NewYork

Tribovillard N, Algeo TJ, Lyons T, Riboulleau A (2006) Trace metals as paleoredox and paleoproductivity proxies: an update. Chem Geol 232:12–32. https://doi.org/10.1016/j.chemgeo.2006.02.012

Wan XQ, Liu WC, Li GB, Li Y (2003) Cretaceous black shale and changes in seawater oxygen content: a case study of southern Tibet. Geol China 01:36–47

Wan HW, Tang LY, Zhang HC, Li CH, Pang YZ (2008) Pollen records and climatic environment in the eastern qaidam basin during the period of 36–18 kaB.P. Quat Sci 01:112–121

Wang FY, Bian LZ, Zhang SC, Zhang BM, Liang DG (2001) Two types of hydrocarbon-generating parent materials in ordovician marine source rocks in the Tarim Basin. Sci Sin (terrae) 02:96–102

Wang YZ, Wu CD, Fang YA, Ma J, Shen B, Huang F, Zhou TQ, Wang JL, Zhang W (2019) Origin and palaeoenvironmental indications of Eocene to Oligocene primary lacustrine dolomite, northern tianshan mountains. NW China. J. Asian Earth Sci 198:104135. https://doi.org/10.1016/j.jseaes.2019.104135

Wang T, Zhu XM, Dong YL, Chen HH, Su B, Liu Y, Wu W (2020) Trace elements as paleo sedimentary environment indicators: a case study of the paleogene anjihaihe formation in the northwestern junggar basin. Acta Geol Sin 94(12):3830–3851. https://doi.org/10.19762/j.cnki.dizhixuebao.2020045

Wang T, Zhu XM, Dong YL, Yang DQ, Su B, Tan MX, Liu Y, Wu W, Zhang YX (2021) Signals of depositional response to the deep time paleoclimate in continental depression lakes: insight from the anjihaihe formation in the northwestern junggar basin. Earth Sci Front 28(01):60–76. https://doi.org/10.13745/j.esf.sf.2020.5.8

Wang KF, Zhang YL, Wu GX, Li YY, He CQ, Zhang HZ (1994) Study on the thermal simulation of oil generation from Pediastrum. J. Tongji Univ. (Nat. Sci.) (02):184-191

Wei W, Algeo TJ, Lu Y, Lu Y, Liu H, Zhang S, Peng L, Zhang J, Chen L (2018) Identifying marine incursions into the paleogene bohai bay basin lake system in northeastern China. Int J Coal Geol 200:1–17. https://doi.org/10.1016/j.coal.2018.10.001

Wersin P, Hhener P, Giovanoli R, Stumm W (1991) Early diagenetic influences on iron transformations in a freshwater lake sediment. Chem Geol 90:233–252

Whitney BS, Mayle FE (2012) Pediastrum species as potential indicators of lake-level change in tropical South America. J Paleolimnol 47(4):601–615

Wignall PB, Myers KJ (1988) Interpreting benthic oxygen levels in mudrocks: a new approach. Geol 16:452–455

Wu J, Li H, Goodarzi F, Min X, Cao W, Huang L, Pan Y, Luo Q (2022) Geochemistry and depositional environment of the mesoproterozoic xiamaling shales, northern North China. J Petrol Sci Eng 215:110730

Xia LW, Cao J, Lee C, Stüeken EE, Zhi D, Love GD (2020) A new constraint on the antiquity of ancient haloalkaliphilic green algae that flourished in a ca. 300ma paleozoic lake. Geobiol 19(2):147–161. https://doi.org/10.1111/gbi.12423

Xiao JY, Wu YS, Zheng MP (1996) A preliminary study on the late quaternary palopollen flora in zabuye salt lake. Tibet Acta Micropalaeontol Sin 04:395–399

Xie XM, Teng GE, Yang YF, Hu MX, Bian LZ (2013) Application of Leica QWinv3 image analysis software in organic petrologic quantitative study. Pet Geol Exp 35(04):468–472. https://doi.org/10.11781/sysydz201304468

Xu CC, Zou WH, Yang YM, Duan Y, Shen Y, Luo B, NiC FuXD, Zhang JY (2017) Status and prospects of exploration and exploitation of the deep oil & gas resources onshore China. Nat Gas Geosci 28(08):1139–1153. https://doi.org/10.11764/j.issn.1672-1926.2017.07.014

Yandoka BS, Abdullah WH, Abubakar MB, Hakimi MH, Adegoke AK (2015) Geochemical characterisation of early cretaceous lacustrine sediments of bima formation, yola sub-basin, northern benue trough, NE Nigeria: organic matter input, preservation, paleoenvironment and palaeoclimatic conditions. Mar Pet Geol 61:82–94. https://doi.org/10.1016/j.marpetgeo.2014.12.010

Yu M, Gao G, Jin J, Ma WY, He D, Xiang BL, Fan KT, Liu M (2022) Hydrocarbon generation simulation of coaly source rocks in the lower combination on the southern margin of junggar basin and indications for oil and gas sources of well gaotan 1. Pet Geol Exp 44(04):687–697

Yu M, Gao G, Ma WY, Liu M, Ni Z, Zhang YJ, He D, Fan KT, Guo LLB, Li J (2023) Hydrocarbon generation differences of shales composed of green algal and cyanobacteria: A case study of Mesozoic and Cenozoic saline lacustrine shales in junggar basin NW China. Pet Sci 20:3348–3362. https://doi.org/10.1016/j.petsci.2023.08.023

Yuan W, Liu GD, Yuan HQ (2023) Discovery of algal fossils in chang-7 organic-rich shale of upper triassic yanchang formation in ordos basin and its geological significance. Geol Rev 69(01):365–374. https://doi.org/10.16509/j.georeview.2022.06.091

Zamaloa M, Tell G (2005) The fossil record of freshwater micro-algae pediastrum meyen (Chlorophyceae) in southern South America. J Paleolimnol 34(4):433–444

Zhang K, Liu R, Liu ZJ, Li BL, Han JB, Zhao KG (2020) Influence of volcanic and hydrothermal activity on organic matter enrichment in the upper triassic yanchang formation, southern Ordos Basin. Central China Mar Pet Geol 112:104059

Zhang YD, Su YL, Liu ZW, Chen XC, Yu JL, Di XD (2015) Long-chain n-alkenes in recent sediment of lake lugu (SW China) and their ecological implications. Limnologica Ecology & Management of Inland Waters.

Zhao W, Wang S, Wei J, Yin DP, Dong CH, Wang Z, Li B (2021) Morphology and taxonomy of genus pediastrum in chlorophyta in beijing area. J Dalian Ocean Univ 36(03):437–445

Zheng RC, Liu MQ (1999) Study on paleo-salinity of chang 6 oil-bearing formation in ordos basin. Oil Gas Geol 01:22–27

Zheng Z, Wang JH, Liu CL, Zou HP, Zhang H, Deng Y, Bai Y (2003) Holocene high-resolution environmental records of shuangchi maar lake. Hainan Island Chin Sci Bull 03:282–286. https://doi.org/10.1360/03tb9105

Zhou CM, Cheng JH, Aaliya A, Shi TM, He CQ (2012) Geological age and paleoenvironmental significance of the upper part of the middle anji haihe formation in the southern margin of the junggar basin, xinjiang. J Stratigr 36(04):723–732. https://doi.org/10.19839/j.cnki.dcxzz.2012.04.006

Zhu HR, Zeng ZQ, Zhang ZY (1978) A preliminary analysis of the fossils of the neogene dainan formation in northern jiangsu and their sedimentary environment. Acta Palaeontol Sin 03:233–244+357

Zhu YH, Zhan JZ, He CQ (2022) Eocene new freshwater dinoflagellate cysts from the lower member of anjihaihe formation, southern edge of junggar basin, xinjiang. Acta Micropalaeontol Sin 39(02):137–145. https://doi.org/10.16087/j.cnki.1000-0674.20220602.001